Estimation and mapping of above ground biomass for the assessment and mapping of carbon stocks in tropical forest using SAR data- a case study in Afram Headwaters Forest, Ghana

Nguyen Thanh Nga

March, 2010

Estimation and mapping of above ground biomass for the assessment and mapping of carbon stocks in tropical forest using SAR data - a case study in Afram Headwaters Forest, Ghana

by

Nguyen Thanh Nga

Thesis submitted to the International Institute for Geo-information Science and Earth Observation in partial fulfilment of the requirements for the degree of Master of Science in Geo-information Science and Earth Observation, Specialisation- Natural Resources Management

Thesis Assessment Board

Prof. Dr.W.Verhoef (Chair), WRS Department, ITC, the Netherlands

Prof. Dr.Ir.R. de Wulf (External examiner), Ghent University

Dr.Y.A. Hussin (1st supervisor), NRS Department, ITC, the Netherlands

Supervisors

Dr.Y.A. Hussin (1st supervisor), NRS Department, ITC, the Netherlands

Dr. M.J.C Weir (2nd supervisor), NRS Department, ITC, the Netherlands

ITC

INTERNATIONAL INSTITUTE FOR GEO-INFORMATION SCIENCE AND EARTH OBSERVATION

ENSCHEDE, THE NETHERLANDS

To My family …

Abstract

Quantifying aboveground biomass (AGB) and carbon sequestration in tropical forests has a significant concern within the UNFCC and Kyoto Protocol for the improvement of national carbon accounting as well as for addressing the potential areas for carbon credits under REDD. The aim of this research is to estimate AGB and carbon stocks for tropical forest using SAR data in Afram Headwater Forest, Ghana.

Two radar images: ALOS PALSAR L band (HH, HV polarisation) and ENVISAT ASAR C band (HH polarisation), both acquired in 2009 were used in this research. An ASTER image acquired in 2008 was under fused with ALOS PALSAR using principal component analysis and IHS transformation in order to obtain the advantages of both in vegetation studies. DBH was measured in 75 plots stratified in three main land-cover types (nature forest, plantation forest and agro-forestry) and then converted to AGB using available allometric equations. The correlation of biomass value measured in each plot and the radar backscatter extracted from different bands and polarisation of radar images, as well as fused data were assessed by the Pearson correlation coefficients. Regression modelling was applied to estimate AGB for the whole study area and the estimated result was validated using validation data collected in the field.

The strongest correlation was identified between L band HV cross-polarization and AGB in the nature forest. Very weak correlations were found in agro-forestry and in plantation forest. Statistical analysis also indicated a poor potential of like-polarized L band and C band in correlation with AGB. Similarly, a weak correlation was found for the radar and optical fused data and AGB. An application of multi-linear regression model of L band cross-polarized and like- polarized radar backscatter for natural forest area showed an enhancement in the relationship with AGB.

The results found in this research agree with previous research in radar application. It indicates the ability of long wavelength cross-polarized radar image to estimate AGB accurately and simply for tropical forests in which optical imagery application are restricted by cloud and weather conditions. It also provides a proof that the fusion of radar and optical image cannot be used to estimate AGB. The unexpected result in plantation forest can be explained by the influence of different management and tree age in plantation forest of the study area. Further research is needed to investigate how strong these factors affect on the relationship between AGB and radar backscatters as well as to develop a appropriate method to estimate AGB and carbon stocks in plantation forest in future.

Keywords: above-ground biomass, estimation, mapping, carbon stock, radar backscatter, cross-polarisation, regression analysis

Acknowledgements

Table of contents

List of figures

List of tables

Abbreviations and Acronyms

AGB	Above-ground Biomass
RMSE	Root Mean Square Error
DBH	Diameter at Breast Height
REDD	Reduced Emissions from Deforestation and Forest Degradation in developing countries
UNFCCC	United Nations Framework Convention on Climate Change
ENVISAT ASAR	Environment Satellite-Advanced Synthetic Aperture Radar
ALOS PALSAR	Advanced Land Observing Satellite Phased Array type L-band Synthetic Aperture Radar
ESA	European Space Agency
FAO	Food and Agriculture Organization of the United Nations
GPS	Global Positioning System
PBC	Pixel-based classification
MLC	Maximum Likelihood Classification
DN	Digital Number
HH	Horizontal Transmit and Horizontal Receive
HV	Horizontal Transmit and Vertical Receive
VV	Vertical Transmit and Vertical Receive
VH	Vertical Transmit and Horizontal Receive

1.   Introduction

1.1.   Background

Green house gas (GHG) emission has been one of the most urgent issues of concern worldwide as the main anthropogenic cause of climate change. Global efforts to reduce the concentration of GHG have been marked by the establishment of international agreements. For instance, the article 4 of United Nations Framework Convention on Climate Change (UNFCCC) mentioned the reduction and prevention of anthropogenic emissions of GHG. The Kyoto Protocol specifically required countries to limit or reduce the directly human induced emissions of GHG.

Forest covers nearly one-third of the earth's land surface and accounts for almost half its terrestrial carbon pool (CPF, 2008). This important role of forest in the global carbon cycle was pointed out in several articles of Kyoto Protocol (Brown, 2002). Among these, the issue of deforestation and degradation of tropical forests, which caused 15-25 % annual global GHG emission, is recognized. Recently, UNFCCC has considered the need to reducing carbon emissions from deforestation and forest degradation in developing countries (REDD) as one of the central efforts to combat climate change (Gibbs *et al.*, 2007). Moreover, the decision 2/CP13 of UNFCCC also mentioned approaches to simulate action for REDD (UNFCC, 2008).

Defined as "organic material both above ground and below ground, and both living and dead, e.g. trees, crops, grasses, tree litter, roots, etc …"(FAO, 2004), biomass is important for many purposes as resource use and environmental management (Chen *et al.*, 2003; IPCC, 2006). Especially, biomass assessment is needed for inferring to carbon sequestration. As the carbon stored in the aboveground living biomass of trees is typically the largest pool, estimating above ground forest carbon and biomass is the most critical step in quantifying carbon stocks and fluxes from tropical forests (Gibbs *et al.*, 2007).

The IPCC Guideline for national Green House Gas inventories (IPCC, 2006) mentioned two ways, directly and indirectly, to derive aboveground biomass. In another research, (Lu, 2006) mentioned approaches to estimate biomass based on field measurements, remote sensing and GIS. Although providing the best accuracy, the traditional techniques based on field measurements are also very costly and time consuming (de Gier, 2003). Satellite imagery based techniques provide an alternative to traditional methods by providing spatially explicit information and enable repeated monitoring, even in remote locations, in a cost-effective way (Patenaude *et al.*, 2005; Rosillo-Calle *et al.*, 2007). With the advantage of capability to provide spatial, temporal, and spectral information (Brown, 2002), remote sensing can of be used as a tool to estimate carbon to meet the requirements of the Kyoto Protocol (Rosenqvist *et al.*, 1999). Additional ground based data collection is required because no remote sensing instrument can measure directly (Rosenqvist *et al.*, 2003).

1.2.   Research conceptual framework

Tropical forest is the second major land cover type in Ghana after the comprising savannas (Blay *et al.*, 2007; Appiah *et al.*, 2009). Therefore, the need for quantification of aboveground biomass and carbon sequestration in these forests has a significant concern within the UNFCC and Kyoto Protocol in general and for the improvement of national carbon accounting as well as addressing the potential areas for carbon credits under REDD for Ghana in particular.

Despite the advantages of less expensive and efficiently accurate measurement (Patenaude *et al.*, 2005), remote sensing methods for biomass estimation are more successful in boreal and temperate forests or young forest with lower forest carbon densities rather than tropical forest (Rosenqvist *et al.*,

2003). Because the carbon rich and the structurally complex ecosystems cause the optical remote sensing signals to be saturated quickly, the tropical forests have been hindered in carbon stock estimation. The sources of uncertainty consist of: lack of completeness, the used model, lack of data, lack of representativeness of data, statistical random sampling error, measurement errors, mis-classification etc. (IPCC, 2006) .

Research on forest and radar remote sensing in the past two decades showed that SAR images with multiple wavelengths, polarizations and incident angles have the potential to extract the needed information of biomass in complex areas such as tropical forests (Henderson and Lewis, 1998). With physically based radar backscatter models and appropriate inversion procedure, it is possible to use multi-frequency polarimetric SAR data to map biomass and overcome the limits imposed by the saturation effect using optical data (Henderson and Lewis, 1998; Fernandez, 2002).

As an inherent characteristic of a radar system, the presence of speckles which produces salt and pepper appearance in the radar image can effect adversely the visual and digital processing of radar imagery. The technique used for extracting the homogenous radar backscatter value from the radar image could strongly affect its correlation with the above ground biomass. Processing techniques like filtering and multi look processing are popular in reducing speckle effects but also cause the loss of the texture information (Fernandez, 2002). Accuracy of results can increase when structure is defined by segmentation of vegetation types (Dobson *et al.*, 1995). The integration of radar and optical sensor data also has the potential to reduce the mixed pixels and data saturation problems and incorporates radar information, and therefore, to improve above ground biomass estimation results (Lu, 2006).

The radar backscatter models can be divided into three groups - physical, empirical and semi – empirical models (Hoekman, 1990). The physical models provide an insight into the relationship of backscatter and structure parameter of the forest which is supportive for other models. The empirical models have been restricted by the lack of physical understanding of the backscatter mechanism. Therefore, semi empirical models seem to be a promising approach to model the above ground biomass. Among these, the classical regression modelling is unbiased in explaining the relation of observed forest biophysical parameters and response value from remote sensing data (Lu, 2006).

1.3.   Research Problem

The lack of information about global biomass due to uncertainties in accuracy and cost has limited our knowledge about global carbon budget and its changes over the years. Therefore, the need for accurate estimation of biomass and carbon stocks in tropical ecosystems with high relevance for understanding the global C cycle, the formulation and evaluation of global initiatives to reduce global warming, and the management of ecosystems for C sequestration purposes (Sierra *et al.*, 2007) implies a demand for precise quantified assessment methods.

1.4.   Research Objectives

This research focused on estimation of Above Ground Biomass (AGB) and carbon stocks for tropical forest using SAR data. The Afram Headwater Forest in Ghana is used as a case study in this research.

Specific objectives:
1- To analyse the relationship between the forest stand parameters (diameter at breast height, tree height, crown cover) and the multi-polarised radar backscatter
2- To analyse the correlation of extracted backscatter value from multi-polarised radar imagery and ABG biomass
3- To assess the geometric sensitivity of extracted backscatter value from radar imagery in the correlation with AGB biomass.
4- To assess the correlation between fusion data of optical and radar images and AGB biomass
5- To estimate and validate the AGB biomass for tropical forest based on regression model
6- To map tropical forest biomass and carbon stocks in the study area.

1.5. Research questions

1- How strong is the relationship between the forest stand parameters (diameter at breast height, tree height, % cover) and the multi-polarised radar backscatter?
2- How strong is the relationship between AGB and the multi-polarised radar backscatter?
3- How sensitive is the extracted backscatter value from radar imagery to its geometry in affecting the correlation with AGB biomass?
4- Is the fused data of optical and radar images correlated with ABG biomass?
5- How accurate can the AGB in this study area be estimated using polarised radar backscatter by regression model?
6- Can forest biomass and carbon stocks be mapped using radar images?

1.6. Research Hypothesis

1- The biophysical parameters have a strong correlation with the cross-polarized radar backscatter.
2- The AGB has a strong correlation with the cross-polarized radar backscatter.
3- The geometric sensitivity affects significantly to the correlation of AGB and radar backscatter.
4- The fused data of optical and radar images does not have a strong correlation with AGB biomass.
5- The AGB can be estimated and mapped using polarised radar backscatter by regression model with reasonable accuracy.
6- Forest biomass and carbon stocks can be mapped using radar images.

1.7. Thesis structure

The thesis comprises seven chapters as follows:

Chapter 1 – *Introduction*: introduces the background, conceptual framework of this research as well as describe research problem, objectives, questions and hypothesis.

Chapter 2 – *Remote sensing approaches to estimate ABG biomass*: briefly reviews the application of remote sensing data for biomass estimation in term of using optical and radar data.

Chapter 3 - *Description of study area*: describes in details the characteristics of study area.

Chapter 4 - *Description of Method and dataset*: defines the methods used in this research to answer research questions and achieve the research objectives as well as provide information about data and materials used in this research.

Chapter 5 - *Results*: summarised the results obtained during the data analysis.

Chapter 6 - *Discussion*: discussed about the result in Chapter 5.

Chapter 7 - *Conclusion*: derive conclusions from the discussion in the previous chapter and links to the research objectives and questions in the first chapter.

2. Remote sensing approaches to estimate AGB

Remote sensing techniques provide an alternative to traditional methods in estimating biomass production or carbon dynamic of forest and plantation. With the abilities of capturing spatially explicit information and repeatable monitoring even in remote area in a cost effective way, these have become popular for estimating growing stock of biomass or its productivity area (Rosillo-Calle *et al.*, 2007).

In past decades, several researches focused on developing the relationships between such structural parameters of forests or plantation such as basal area, biomass, crown cover, tree height or diameter at breast height (DBH) and the response value of the electromagnetic radiation. The comparison of these relationships in different types of forest stand structures and environment conditions (soil moisture, species, crown geometry, canopy structure, etc.) is effective to evaluate the forest potential in biomass production. Despite that, the lack of a clear understanding in the relationship of these parameters and reflected value from satellite images caused poor results. However, significant developments in technologies recently have allowed a more accurate measurement at a lower cost that would support researcher to face this challenge.

In this chapter, the application of remote sensing for biomass estimation will be described and reviewed in terms of data from different sensors used.

2.1. Applications of optical remote sensing

2.1.1. High spatial resolution of optical remote sensing

With growing demands for detailed forest information, high spatial resolution remote sensing has become a valuable source of information for assisting forest management (Culvenor, 2003). The term "high spatial resolution" is subjective depending on the context of application. Here, it is refer to both airborne (digital aerial photograph) and space-borne such as IKONOS and QuickBird with spatial resolution less than 10 m (Wulder, 1998).

Fine or high spatial resolution remote sensing data are frequently used for modelling tree parameters or forest canopy structures (Lévesque and King, 2003). Many approaches have been used to extract biophysical parameters from this type of data summarized by (Culvenor, 2003) which are bottom - up algorithm (valley-following and directional texture), a top-down algorithm (multi- scale edge segments, threshold-based spatial clustering, a double-aspect method, and vision expert system), and template matching (Lu, 2006).

The advent of aerial photography catered to the basic requirement of location capabilities and is one of the most widely used forms of remote sensing of forest cover. The applications of aerial photography are the simplest and the oldest forms of aerial sensors used for remote sensing of the earth's surface features. Cameras can be of different types, namely single lens mapping, multiple lens mapping, panoramic and digital. The spatial resolution of camera lenses is more important than spectral information (Rosillo-Calle *et al.*, 2007). The usage of aerial photograph has both advantages and disadvantages which are summarized in Table 2-1 below.

Interpretation of aerial photographs has been used for wide range of applications such as the one related to forest inventory since the late 1940s. This technique has proven useful, especially for stratification and timber volume estimation. Photo interpretation can measure various forest characteristics, such as tree height, crown diameter, crown closure, and stand area. For example, (Tiwari and Singh, 1984) used aerial photographs and non-harvest field sampling for forest biomass

mapping in India. (De Jong *et al.*, 2003) used digital airborne imaging spectrometer (DAIS) data to estimate biomass using stepwise linear regression analysis in southern France.

Table 2-1 Advantages and disadvantages of the use of aerial photographs - (Rosillo-Calle *et al.*, 2007)

Adavantages

- covers a large area of the land at approximately the same scale;
- high resolution;
- better interpretation of features with stereoscopic vision;
- can be used for places which are ordinarily inaccessible;
- easy to make copies and store;
- easier availability of conventional photographs;
- measurements are possible if the scale is known;

Disadvantages

- absence of geo-referencing makes digitization difficult;
- may have tilts and errors, such as relief displacement;
- positional location and scale are approximate;
- ground features may be obscured by other features;
- lack of contrast in colours;
- cost can prove to be high for small-scale projects;
- relatively long time required to obtain final prints.

Techniques used for extraction of biophysical parameters from aerial photography can also be used in high spatial-resolution satellite images (Rosillo-Calle *et al.*, 2007). An overview of high resolution satellite is shown in Table 2-2.

The fine spatial resolution and associated multi-spectral characteristics may become an important data source for AGB estimation such as in research of (Thenkabail *et al.*, 2004), which used IKONOS data to estimate AGB of oil palm plantations in Africa. It also can be useful as reference data for validation or accuracy assessment for medium and coarse spatial-resolution data applications.

Table 2-2 Overview of high resolution satellite (Rosillo-Calle *et al.*, 2007)

Satellite	Type of sensor	Resolution
CARTOSAT-1 (IRS-P5)	Panchromatic	2.5m
RESOURCESAT (IRS-P6)	LISS IV	5.8m
EROS A1	Panchromatic	1.8m
IKONOS	Panchromatic	1m
	Multispectral	4m
IRS-1C	Panchromatic	5.8m
IRS-1D	Panchromatic	5.8m
QuickBird	Panchromatic	0.61m
	Multispectral	2.44m
SPIN 2	Panchromatic	2m
	Panchromatic	1m
OrbView 3	Multispectral	4m

However, (Lu, 2006) already indicated the drawbacks of using this type of data: high spectral variation and shadows caused by canopy and topography which create difficulties in developing AGB

estimation models; the lack of a shortwave infrared image, which is often important for AGB estimation; the need for large data storage and the time required for image processing prohibit its application in large areas and, last but not least, much more expensive cost , and time requirement to implement data analysis than medium spatial resolution images.

2.1.2. Medium resolution of optical multi-spectral remote sensing

Optical remote sensing is a passive sensing system, using visible and near- infrared reflectance from the earth, which forms the basis for most of current global scale mapping. Optical measurements have been widely used in studies that link AGB measurement from the field to satellite observation that based on the sensitivity of the optical reflectance to variations in the canopy structure. But these measurements have not proven to be consistent over large areas because surface conditions may change more rapidly than the repeat time of the cloud free satellite observations and producing artefacts in the derived maps (Scott *et al.*, 2009).

Optical remote sensing makes use of visible, near infrared and short wave infrared sensors to form images of the earth's surface by detecting the solar radiation reflected from targets on the ground. Different materials reflect and absorb differently at different wavelengths. Thus, the targets can be differentiated by their spectral reflectance signatures in the remotely sensed images.

Optical sensors are characterized by spectral, radiometric and geometric performance. Satellites are usually classified according to their spatial resolution into environmental satellites (Meteosat, GOES, NOAA), medium-resolution satellites (Landsat MSS, IRS1, JERS1); and high resolution satellites (Landsat TM, SPOT, ERS-1, IKONOS, etc.).

The time-series Landsat imagery has become the primary source in many applications, including AGB estimation at local and regional scales (Sader *et al.*, 1989; Roy and Ravan, 1996; Fazakas *et al.*, 1999; Nelson *et al.*, 2000; Steininger, 2000; Mickler *et al.*, 2002; Foody, 2003; Phua and Saito, 2003; Calvatildeo and Palmeirim, 2004; Zheng *et al.*, 2004; Lu *et al.*, 2005). The major approaches include linear or nonlinear regression models, K nearest-neighbour, and neural network (Lu, 2006).

Spectral signatures or vegetation indices are often used for AGB estimation. Most studies involve deriving a relationship between a commonly used vegetation index such as NDVI (normalized difference vegetation index) with biomass or some forest biophysical parameter. A large number of protocols can be used to develop biomass estimates (Rosillo-Calle *et al.*, 2007). Vegetation indices have been recommended to remove variability caused by canopy geometry, soil background, sun view angles, and atmospheric conditions when measuring biophysical properties (Elvidge and Chen, 1995; Blackburn and Steele, 1999). However, not all vegetation indices are significantly correlated with AGB. In general, vegetation indices can partially reduce the impacts on reflectance caused by environmental conditions and shadows, thus improve correlation between AGB and vegetation indices, especially in those sites with complex vegetation stand structures (Lu *et al.*, 2004).

Image texture also has shown its importance in AGB estimation (Lu *et al.*, 2005; Lu, 2006). Individually, pure image textures or spectral responses are insufficient to establish highly accurate AGB estimation models. A combination of spectral and spatial information extraction techniques shows promise for improving estimation performance of forest stand parameters (Wulder, 1998; Lu and Batistella, 2005).

Different degrees of success for AGB estimation have been obtained in previous research. (Foody *et al.*, 2001) found that neural networks were useful for the AGB estimation using Landsat TM data in a Bornean tropical rain forest. In Finland and Sweden, Landsat TM data were used to estimate tree volume and AGB using the K nearest-neighbour estimation method (Halme and Tomppo, 2001). (Nelson *et al.*, 2000) analysed secondary forest age and AGB estimation using Landsat TM data and found that AGB cannot be reliably estimated without the inclusion of secondary forest age. The complex forest stand structure, the impact of shadows caused by canopy and topography, and the

complex environments influence AGB estimation performance (Steininger, 2000; Lu and Batistella, 2005).

Research in the moist tropical forest in the Brazilian Amazon has indicated that image textures are more important than spectral responses for AGB estimation in the forest sites with complex vegetation stand structures (Lu and Batistella, 2005). However, in the forest sites with relatively simple vegetation stand structure, spectral signatures play a more important role than image textures. The roles of spectral responses and image textures in AGB estimation depend on the characteristics of the study area, i.e. the complexity of forest stand structure(Lu *et al.*, 2005). One critical step is to identify suitable image textures that are strongly correlated with AGB but are weakly correlated with each other. Identifying suitable image textures involves the determination of appropriate texture measures, moving window sizes, image bands etc. (Chen *et al.*, 2004). Not all texture measures can effectively extract biomass information because image textures vary with the characteristics of the landscape under investigation and images used. More research is needed to develop techniques for identification of suitable image textures for biomass estimation (Lu and Batistella, 2005).

2.1.3. Hyperspectral optical remote sensing imagery

Imaging spectroscopy or hyperspectral remote sensing is defined as the simultaneous acquisition of images in hundreds relatively narrow, contiguous and/or non-contiguous spectral bands throughout the ultraviolet, visible and infrared portions of the spectrum, facilitating greatly detailed study of the earth's resources (Rosillo-Calle *et al.*, 2007). Therefore, data can be acquired anywhere, globally, at low cost to the end user. Space-borne sensors can provide year-round temporal data.

A review from (Treitz and Howarth, 1999) stated that emphasis applying hyperspectral remote sensing in vegetation studies was placed on monitoring and estimating biophysical parameters which related to forest ecosystem processes and health since this is seen as the area of greatest potential contribution. Narrow-wavelength image could be possible to reduce the saturation problem in biomass estimation (Mutanga and Skidmore, 2004). Thus, hyperspectral imagery with large number of spectral bands with very narrow wavelengths may improve AGB estimation performance (Lu, 2006). The main benefits to end-users are that space-borne hyper-spectral data can provide more detailed and accurate forest inventory information, as well as such specialized products as geo-coded maps of forest biomass or above-ground carbon maps(Rosillo-Calle *et al.*, 2007).

However, there needs to be a consideration among spatial, spectral and radiometric resolutions in hyperspectral remote sensing due to the constraint in data volume (Lu, 2006) and technique difficulties of collecting, storing and processing hyperspectral scanner data (Treitz and Howarth, 1999).

2.2. Application of radar remote sensing for biomass assessment

Radar (radio detection and ranging) is an active system which emits radio waves and illuminates the surface of the earth and records the energy backscattered from the terrain. 'Side-looking airborne radar' (SLAR), can obtain images over vast regions to the left or right of the aircraft, two types of which being used, 'real aperture radar (RAR)', and currently the 'synthetic aperture radar (SAR)' based on whether the antenna being used is of fixed or variable length, respectively (Rosillo-Calle *et al.*, 2007). Characteristics of some selected spaceborne SAR systems can be found in the Table 2-3 below. The most commonly used wavelengths in imaging radar are K (1.19–1.67 cm), C (3.9–7.5 cm), S (7.5–15.0 cm), L (23.5, 24.0, 25.0 cm) and P (30.0–100 cm).

Radar plays a major role for vegetation studies for two reasons: (1) the unique property of microwave remote sensing systems to function almost unimpeded by adverse atmospheric conditions (which prevent the use of optical systems) and (2) the property of (coherent) microwaves to enable measurement of certain object parameters which cannot be assessed through other remote sensing systems (Hoekman, 1990).

Table 2-3 Characteristics of selected Spaceborne SAR systems

Characteristic	ERS-2	JERS-1	Radarsat 2	Envisat -1	ALOS PALSAR
Launch date	04/21/95	02/11/92	12/14/07	03/01/02	01/24/06
Waveband	C-band	L-band	C-band	C-band	L-band
Polarisation	VV	HH	HH,VV,HV,VH	HH,VV,HV,VH	HH,VV,HV,VH
Look angle (degrees)	23	35	10-60	14-45	18-55
Resolution (m)	30	18	3-100	30-1000	10-100

In order to exploit the use of radar backscatter to determine ABG biomass of forest stand, the relationship between radar backscatter and forest stand parameters (diameter at breast height, tree height, Basal area, and stand diversity) is investigated in several studies (Hussin *et al.*, 1991; Le Toan *et al.*, 1992; Beaudoin *et al.*, 2004). Research also showed the capability of SAR image in discriminating various types of forest (Wu, 1990; Van der Sanden, 1997). The relationship between X- and C- band backscatter and stand parameters is quite poor (Hoekman, 1990). The table 2-4 below presented some examples of radar application.

Table 2-4 Selected studies on radar applications adapted from (Lu, 2006)

Radar dataset	Study area	Techniques	Reference
SIR-C	South – eastern USA	Multiple regression analysis	(Harrell *et al.*, 1997)
SAR L band	Les Landes Forest, France	Adapted theoretical model	(Beaudoin *et al.*, 1994)
AIRSAR C,L,P band	Freiburg, south-east Germany; Ruotsinkyla, Finland	Linear regression analysis	(Rauste *et al.*, 1994)
JERS-1 SAR L band	Tapajos, Para state and Manaus, Amazonas state, Brazil	Forest backscatter model	(Luckman *et al.*, 1998)
JERS-1 SAR L band	New South Wales, Australia	Linear regression analysis	(Austin *et al.*, 2003)
AeS-1 SAR P- band	Tapajos River region, Para state, Brazil	Regression models (logarithmic and polynomial function)	(Santos *et al.*, 2003)

Measuring the orientation (polarisation) of the transmitted and received electromagnetic waves allows for further sensitivity to AGB measurements. Extensive analyses with existing SAR sensors, mostly L band, suggest the sensitivity of radar backscatter saturation around 100-150 ton/ha (13) (Scott *et al.*, 2009). HV (horizontal–vertical) polarization in longer wavelengths (L or P band) is most sensitive to biomass (Le Toan *et al.*, 1992) because it originates mainly from the canopy volume scattering and trunk scattering, and is less affected by the ground surface. Reflection from soil and ground may sometimes be recorded as part of the backscatter but can be overcome by using appropriately transformed models (Rosillo-Calle *et al.*, 2007).

The availability of multi frequency or multi polarization data provided by airborne or satellite systems has brought the capability to separate forest types and improve the radar classification (Cronin, 2004).

The studies in the combination of high and low frequency showed promising results, especially for tropical forests (Van der Sanden, 1997). A higher level of biomass and more accurate results can be achieved by using P band combined with C band or L band for a certain type of forest (Ranson and Sun, 1994; Fernandez, 2002; Cronin, 2004).

In general, above ground biomass can be estimated using with difference approaches in models (directly as linear or non-linear regression models, neural network and K nearest neighbour or indirectly as canopy reflectance models), spatial resolutions (fine, medium, coarse) or types of remote sensing data (optical, radar or Lidar) (Lu, 2006). Each of these approaches relies on the calibration of remote sensing measurement and the in situ estimation of above ground biomass, mostly by using a combination of allometric relationships of simple plot-level measurements and AGB (Scott *et al.*, 2009).

Reflection from soil and ground may sometimes be recorded as part of the backscatter but can be overcome by using appropriately transformed models (Rosillo-Calle *et al.*, 2007). There are different kinds of backscatter models, namely, radiative transfer models, regression models and conceptual models. These models considered the effect of general canopy and terrain characteristics to predict the value of radar returned (Fernandez, 2002). The scattering behaviour of the waves is decompressed according to interaction models (Ulaby *et al.*, 1990) . Because of the high degree of complex interaction, the inversion of scattering models for estimation or prediction biomass directly is still not possible (Fernandez, 2002).

The saturation problem is a common problem in radar data (Balzter, 2001). The saturation levels depend on the wavelengths (i.e. different bands, such as C, L, P), polarization (such as HV and VV), and the characteristics of vegetation stand structure and ground conditions(Lu, 2006).

2.3.   Application of Lidar remote sensing data

'Laser' is an acronym for 'light amplification by stimulated emission of radiation'. It is another type of active remote sensing sensor. The laser sensor system used for remote sensing is called 'lidar' (light detection and ranging) (Rosillo-Calle *et al.*, 2007). Like radar, lidar is based on the concept of actively sensing the vegetation using a pulse of energy, in this case from a laser operating at optical wavelengths (rather than at radio wavelengths) (Scott *et al.*, 2009).

Lidar is an active system offering tremendous potential for monitoring forest biomass with the major advantage as the acquisition of three-dimensional data of the forest structure, and data on canopy cover characteristics, leaf area index, crown cover and volume, etc. The ability of the laser altimeters to penetrate forest canopies through to the ground level is a further benefit (Rosillo-Calle *et al.*, 2007).

Previous research has indicated that use of lidar data is a promising approach for biophysical parameter estimation (Drake *et al.*, 2002; Hyde *et al.*, 2005). Lidar data alone, as well as in combination with other sensor or ancillary data, will provide an important data source for forest parameter estimation. Examples of the application of lidar data to forest studies includes: estimate timber volume (Næsset, 1997) and stand height (Næsset, 1997), estimate tropical forest biomass (Drake *et al.*, 2002), Douglas fir western hemlock biomass (Lefsky *et al.*, 1999), temperate mixed deciduous forest biomass (Lefsky *et al.*, 1999), tree height and stand volume (Nilsson, 1996), tree crown diameter(Nilsson, 1996), and canopy structure (Lovell *et al.*, 2003). Long-wavelength radar data have the advantage in AGB estimation for complex forest stand structure and lidar data have the potential to provide vertical structure information(Zimble *et al.*, 2003).

However, the lidar data were captured through airborne sensors which cost more than spaceborne (Lu, 2006). Moreover, the complexity of data analysis requires skills, knowledge and specific software. As a result, applications of lidar were only in typical study areas and not extensive to AGB estimation in regional and global scale yet.

2.4. Constraints and difficulties for remote sensing application in biomass assessment

Remote sensing has developed into an important tool for monitoring and evaluation, and as a subsequent decision-making tool for various bioenergy and carbon sequestration projects. The feasibility of the use of remote sensing for monitoring of carbon stocks and flows in a project has been assessed by (Vine *et al.*, 1999).

Finding an optimum combination of accuracy of measurements and the cost of the technology is often a major challenge in projects using remote sensing for estimating forest or plantation biomass and carbon sequestration. Among the remote sensing techniques available, estimation of biomass and detection of biomass change can be best achieved using SAR data. Studies have shown that SAR data can detect the half of the tree trunks removed by selective logging. Modelling biomass production or carbon sequestration, however, needs both optical and SAR data to be combined. Changes in land use can be obtained only by optical data (Scott *et al.*, 2009). No single sensor or any satellite mission, whether radar, lidar or optical, can be expected to provide consistently infallible estimation of biomass but use of these measurements in a synergistic fashion can potentially overcome the limitation of each (whether radar saturation, lidar sampling modes or optical temporal matches).

Quantification of the uncertainties associated with biomass calculations and optimization of remote sensing techniques to reduce uncertainties is required. Considerations of issues of accessibility and affordability of data should be addressed at global and particularly project scales.

3. Description of the study area

Due to the availability of such characteristics of a typical tropical forest in Africa and the data (map and remote sensing data), accessibility, the chosen study area for this research was Afram Headwater Forest Reserve. This chapter describes briefly main characteristics of this study area in terms of location, topography, climate, etc.

3.1. Geographic location and settlement

The Afram Headwaters Forest Reserve extends from $1^o32'$ W to $1^o48'$W and $6^o45'$N to $7^o25'$ N in Offinso District, Ashanti region of Ghana. The Kumasi- Techiman trunk road which links the northern part of Ghana to the Southern part run through the eastern part of the reserve. The northern part is linked to Sekye Dumasi district with the capital in Ejura which is one of the largest agriculture towns noted for cultivating yam and maize in the country. With the size of 20100 hectares, this area is within the transaction zone of forest and savannah, comprising both natural and plantation forest, and legal farms which are admitted by the Reserve Committee. Figure 3-1 showed location map of the study area.

Figure 3-1 Ghana and a zoom to the Afram Headwaters Reserve in Google Earth

The communities living in this area are predominantly migrant people who depend on the forest reserve for their livelihoods. They are engaged in various forms of activities such as farming, hunting, palm wine tapping and livestock rearing. The traditional farming practice as slash and burn is one of the main reasons causing the area turning to grassland and high vulnerable to fire. There are five towns near the boundary of the reserve: New Offinso (36,190 people), Akomadan (14,018 people), Abofour (11,177 people), Nkenkaasu (10,014 people) and Afrancho (7,727 people). The main religious groups are Christians, Islam and Traditional Religion.

3.2.   Topography and drainage

Figure 3-2 Slope map (generated from geological dataset of Ghana

The topography of this area is relatively flat or gently undulating with the altitude ranging from 300 m to 400m above the sea level. The slope mostly is less than 5%, some from 5% to 10%. However, some limited areas in the eastern part have steeper slopes (from 10-15%).

The two main streams in the area are the Afram in the east and the Brimu in the west part of the study area. One of the main roles of Afram Headwater reserve is to protect these major water sources for domestic and industrial consumption for the whole district of Offinso.

3.3.   Climate

With the semi-equatorial conventional climate, the study area has two rainfall seasons: the major one from April to July and the minor one from September to mid November. This results in a high annual rain fall ranging from 1500 mm to 1700mm. Relative humidity is generally high (around 80%). The maximum temperature is 30°C in March and April and average monthly temperature is about 27°C. Prevailing winds are south-westerly during wet season and north easterly during dry season. Table 3-1 showed the average temperature and rainfall in the study area over 7 years (from 2000 to 2007). During the dry season from December to March, forest fires usually happen in this area.

Table 3-1 Average temperature and rainfall in Afram Headwater Reserve (2000-2007)

	Jan	Feb	Mar	April	May	June	July	Aug	Sept	Oct	Nov	Dec
Max temp. (^{o}C)	32.8	33.8	33.9	32.6	31.8	30.1	28.7	28.1	29.4	31.1	32.0	31.8
Rainfall (mm)	35.2	42.6	114	170	170	190	143	68.8	188	189	61	27.4

3.4.   Geology and geomorphology

The main geological type is sandstone which accounted for 70% study area. Granitoid only remains in the 20% area of the North Western part. While as, the smallest area in the South has Phyllite, Schist, Tuff and Greywacke. The western part of the area overlies with the upper and lower Birrimian series while elsewhere the area overlies with the voltaic sandstones. The geological map of the study area is shown on Figure 3-3.
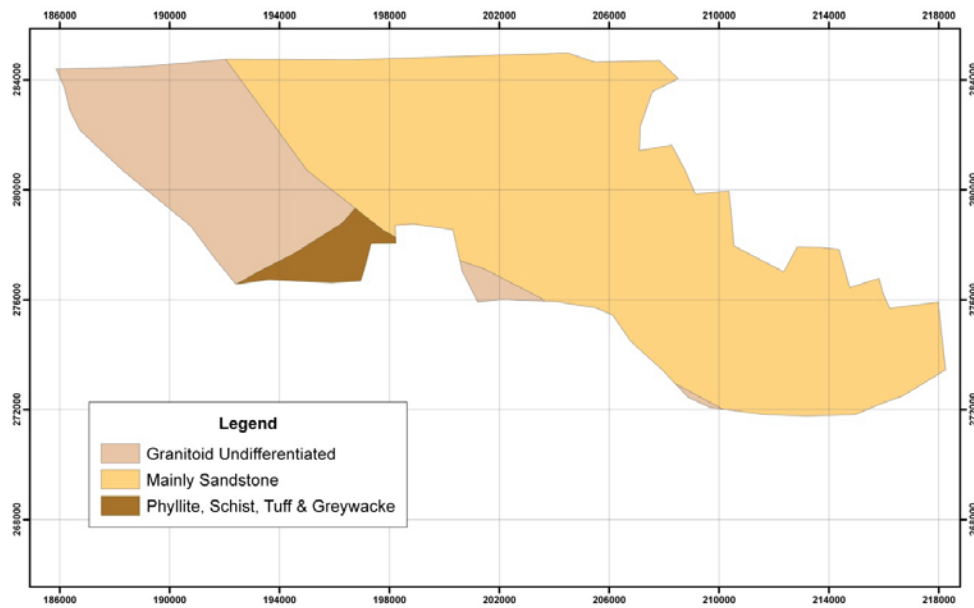
Figure 3-3 Map of Geological types (created from geological dataset of Ghana)

3.5. Soils

Soil is generally uniform with most of the reserve consisting of reddish brown sandy loams and occasionally patches of clay do sometimes occur. Main soil types in the study area include: Acrisol, Leptosol and Lixisols which are shown in the soil map of Afram Headwater reserve in Figure 3-4.
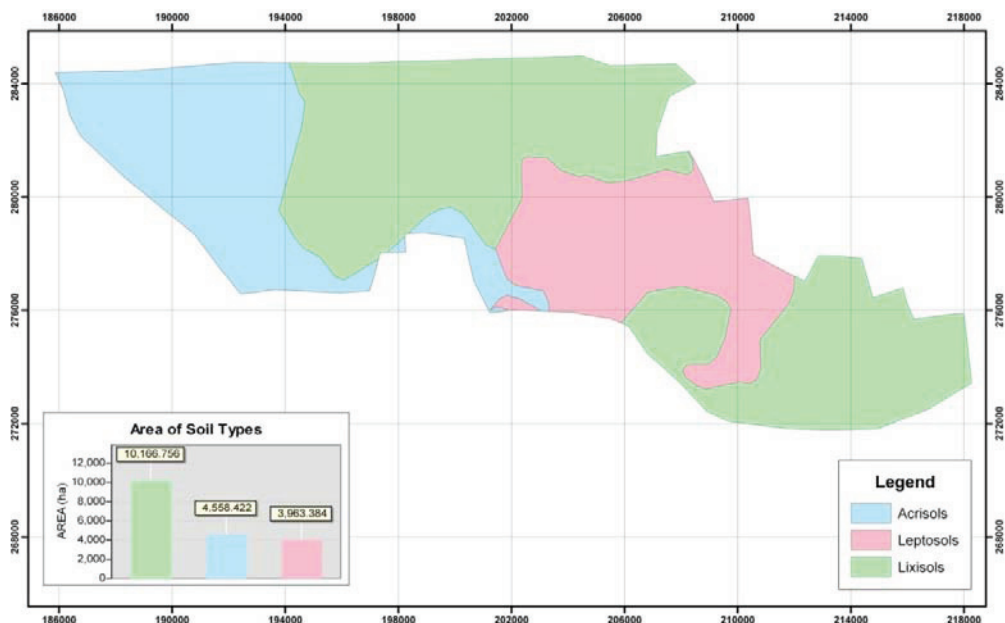
Figure 3-4 Soil map (generated from geological dataset of Ghana)

Acrisol is clay-rich and associated with humid, tropical climates. This type of soil often supports forested areas. Acrisol is common in the West area of Afram Headwater Forest while Leptosols of soil remains in the Southern East of the study area. This is a very shallow soil that is extremely gravely and/or stony. These soils are particularly common in mountain regions. Leptosols are unattractive soils for agriculture. They could have some potential for tree crops or extensive grazing. Leptosols are best kept under forest.

Lixisols are soils with subsurface accumulation of low activity clays and high base saturation. They develop under intensive tropical weathering conditions. This type has the largest area among the three and distribute in the North and East part of Afram Head water forest (FAO, 2003).

3.6. Vegetation cover

The vegetation cover in this study area is moist dry deciduous forest. The forest inventory report for 1987 identified 173 different species of trees. The forest reserve is described to be of high biological diversity and economically valuable in terms class1 timber species. The last forest inventory in 2000 scored the condition of the forest as highly degraded and required human intervention to restore the forest.

There are four types of vegetation cover in this study area: Natural forest, Plantation, Agro-forestry and Fallow land which are defined by (FAO, 2000). In this research, only the first three types will be dealt with.

Natural forest

The Natural forest inside the reserve contributes a small proportion to the area of the whole reserve compared to the area of plantation and taungya system. Most of the forest is degraded with the invasive York (*Musanga Cecropoides*). Figure 3-5 showed images of natural forest from the field trip. The list of main native trees in the forest can be found in Appendix-A.

Broussonetia Papyrifera (Paper mulberry) is one of the most serious non-indigenous woody invasive plants. The high concentration of paper mulberry in Afram Headwater forest was caused by extensive deforestation and bushfires. It is locally known as 'York' the name of the technical officer who worked on the plots during the1970s.
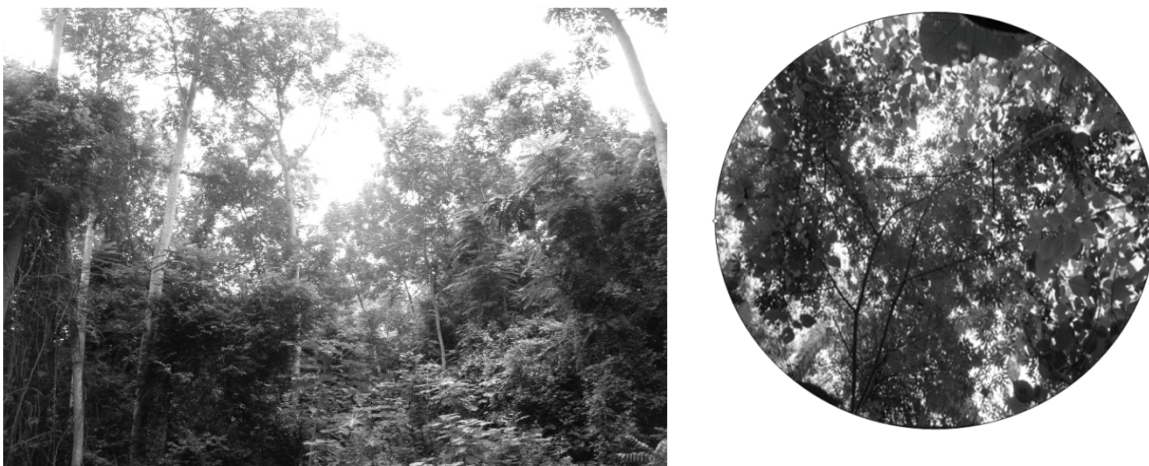
Figure 3-5 Images of natural forest from field work trip (left: secondary forest, right: crown cover of dense York)

Plantation forest:

The study area has experienced repeated burning as a result of accumulation of debris from timber havesting in the past. The burnt forest is dominated by pioneer trees of little economic merit and is more prone to fire in future. Consequently, part of the reserve is converted to plantation. There are on-going restoration programs in the reserve through plantation establishment by the monoculture of exotic tree species such as cedrela (*Cedrela odorata*) and teak (*Tectona grandis*) and mixed stands of local tree species. Figure 3-6 showed images of teak plantation and its crown cover taken from the field area.
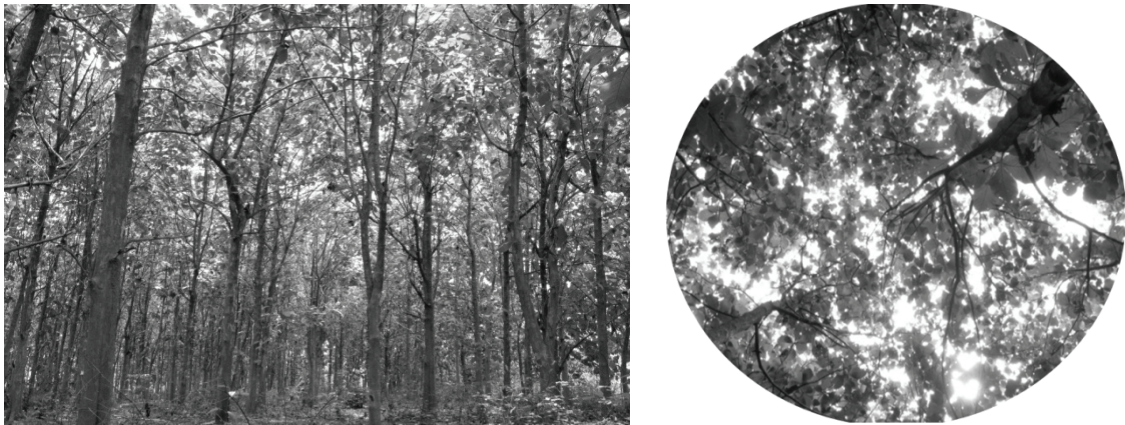
Figure 3-6 Images of plantation forest from field work trip (left: teak plantation, right: crown cover of teak)

Agro-forestry

Agro-forestry is a collective name for land use system and practices where woody perenial are deliberately integrated with crops and/or animalson the same land management unit. The integration can be either in spatial mixture or temporal sequence. There are normally both ecological and economic interaction between the woody and non-woody component in agro-forestry (Schoene *et al.*, 2007). Images of agro-forestry in the study area were shown in Figure 3-7 below.

Figure 3-7 Images of agro-forestry from field work trip

The plantation development program mainly employed taungya system in which farmers are given parcels of degraded forest reserve to produce food crop and help establish and maintain tree resources. The main crops are yam, cocoyam, maize, cassava, plantain, okra, palm trees (see appendix C). Besides, in perennial cropping system in which land was put under plantation of cocoa, oil palm, rubber, teak and wood lots which take more than 1 year to mature. The native trees here are left for shading for trees in seedling and sapling stages.

Fallow land

This type of land cover predominant under the cover of *Pernnisetum purprureum* (elephant grass) and other tall grasses that grow up to about 3-4 m high. There are two types of fallow land in the study area. Old fallow land which is lands intensively logged or farmed in the past and now left for regeneration into secondary forest (5-10 years) have more trees and less herbaceous and shrubby materials and less susceptible to wild fire. The young fallow lands which are agriculture lands that lost fertility and abandoned to regain fertility for 4 years. It has herbaceous and shrubby materials for example *chromolaena odorata* which is susceptible to impact of wild fire and influence forest regeneration.

Figure 3-8 Images of fallow land in Afram Headwaters

4. Description of method and data used

The main purpose of this chapter is to describe methods and data used in this research.

4.1. Method

The method to carry out the research is described in the following flowchart:
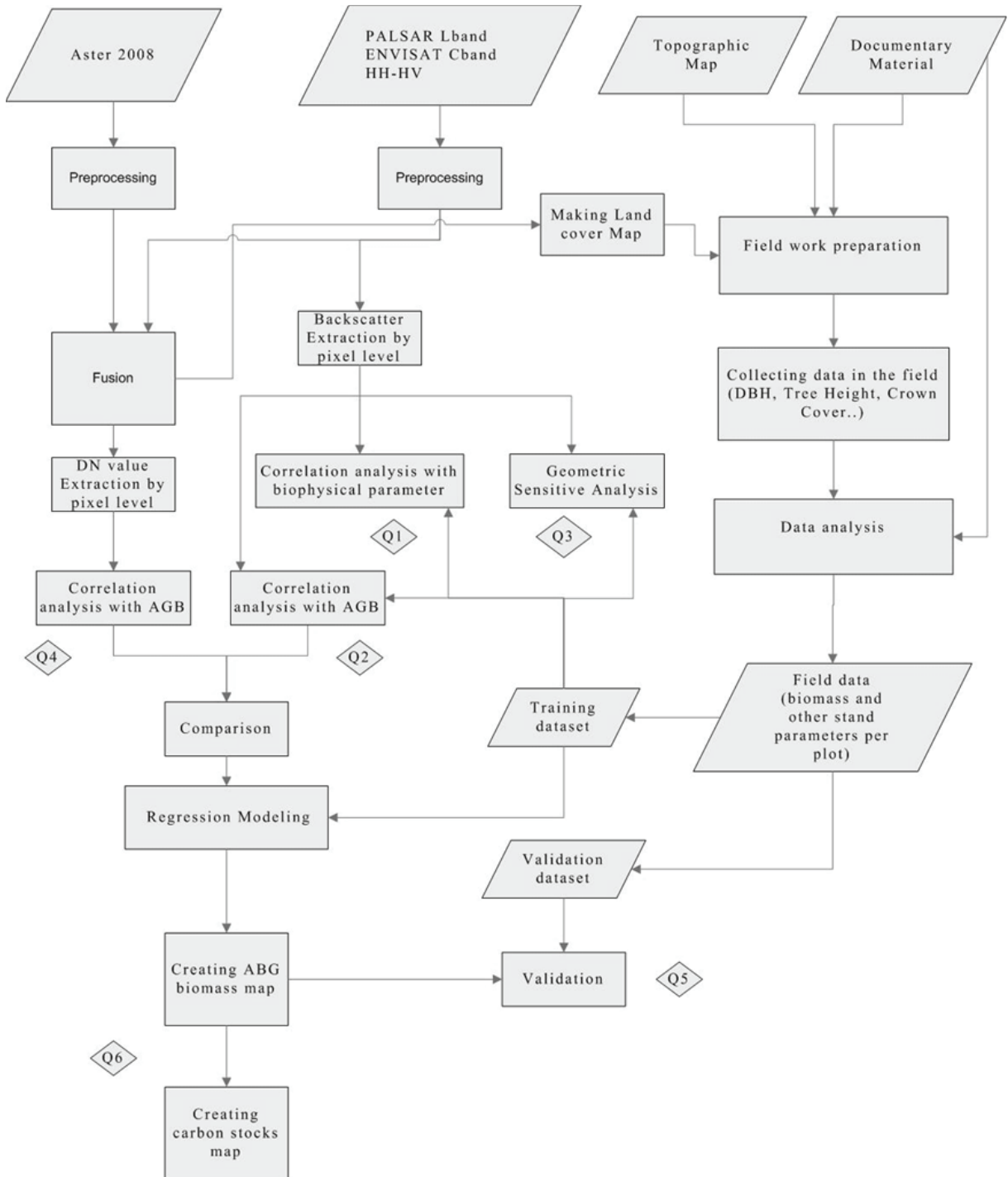
Figure 4-1 Methodology flowchart

4.1.1. Pre-processing of optical data

The pre-processing procedure aims to correct distorted or degraded image data to create more faithful representation of the original scene. This typically involves the initial processing of raw data to correct for geometric distortions, to calibrate the data radiometrically and to eliminate noise present in the data (Lillesand *et al.*, 2004).

The intent of the geometric correction is to compensate for the distortions introduced by paranomic distortion, earth curvature, atmospheric refraction, relief displacement and nonlinearities in the sweep of sensor IFOV. Geometric correction process normally implemented as two steps considering systematic distortion (by applying formulas derived by modelling the source of distortion) and random distortions (by analysing well distributed ground control points (GCPs) occurring in an image) (Lillesand *et al.*, 2004).

The radiance measured by the any given system over a given object is influenced by such a factor as changes in scene illumination, atmospheric conditions, viewing geometry and instrument response characteristics. Sun elevation correction and earth-sun distance correction was carried out for mosaics purpose of images taken at different times or studying the changes in reflectance of ground feature at different times or location. Atmospheric correction reduces the influence of atmospheric effects to solar illumination variation (Lillesand *et al.*, 2004).

The Aster image adapted from ITC was already pre-processed and geo-referenced to the UTM – WGS 84 coordinate system. To project in Ghana coordinate system, it was rectified to the Ghana topographic map using Arc GIS software.

4.1.2. Pre-processing of radar data

To process and extract information from SAR imagery, pre-processing has to be done first to remove radiometric and geometric distortions. Since SAR transmits and receives from one side of the satellite, the return signal bounces off and returns from objects on the ground nearer to the satellite more quickly than those further away. This slight delay in return affects the strength of the return beam, creating a radiometric distortion, or unevenness in the energy measurements.

Radiometric calibration of SAR is defined by (Curlander and McDonough, 1991) as the process of characterising the performance of the end to end SAR system in term of its ability to measure the amplitude (and phase) of the backscattered signal. The need for calibration depends on the intended data analysis method. Application with a quantitative analysis approach often aims to compare backscatter measurements so that calibration is required (Van der Sanden, 1997).

The process of calibration can be separated into a lower process (relative calibration) and a higher level process (absolute calibration). Relative calibration provides a common basis for all image pixels. A good relative calibration will permit repeatable backscatter measurement in both space and time. A good absolute calibration will result in backscatter measurements that are both repeatable and accurate (Van der Sanden, 1997).

Speckle, a salt and pepper (very high and very low values) appearance on SAR imagery is a common radiometric distortion. It is caused by the reflective objects on the ground, positioned in such a way that their reflected wave either positively interfere with each other, creating a very bright return- or negatively interfere, creating a dim return. Gamma, Lee and Frost filters are often employed to minimize this effect (PCI-Geomatics, 2009). The speckle reduction is not carried out here to maintain the texture information and will be dealt later with the idea of using the convolution filtering in Erdas software.

The next step in SAR processing is generally removing geometric distortions. Radar images suffer from significant geometric distortion because they are acquired in a slant range. This slanted image

geometry creates carrying pixel dimensions across track, with the worst distortion occurring closer to the radar platform. Using a DEM and a computed math model, radiometric terrain correction diffused and stretches the return from the slopes facing the sensor (restores mean energy level) and concentrates and compresses the return from the back slopes, restoring radiometric uniformity to the image (PCI-Geomatics, 2009).

Once the radiometric and geometric distortions have been removed, the radar image is registered or spatially related, to other images, a specified coordinate system or GIS base map (Rosich and Meadows, 2004). Since the ALOS PALSAR and ENVISAT ASAR obtained from ITC was pre-processed, only the geometric rectification to local coordinate system is carried out. The DN value was converted to radar backscatter using specific equations for different type of sensors.

For ALOS PALSAR, the following equation (Shimada *et al.*, 2009) for product level 1.5 was used

$$NRCS(dB) = 10 * log10(DN^2) + CF$$

Where NRCS: normalized radar cross section

DN: Digital number value

CF: Calibration factor

The equation from (Rosich and Meadows, 2004) was used to converted DN value of the ENVISAT ASAR image to backscatter coefficient

$$\sigma_{i,j}^{o} = 10 * log_{10}\left(\frac{DN_{i,j}^2}{k} sin(\alpha_{i,j})\right)$$

Where $\sigma_{i,j}^{o}$: backscatter coefficient for pixel (i,j)

$DN_{i,j}$: Digital number value at pixel (i,j)

k: Absolute calibration constant

$\alpha_{i,j}$: Incident angle

4.1.3. Data fusion of radar and optical imagery

Data fusion is an effective way for optimum utilization of large volumes of data from multiple sources. Multi-sensor data fusion seeks to combine information from multiple sensors and sources to achieve inferences that are not feasible from a single sensor or source. The fusion of information from sensors with different physical characteristics enhances the understanding of our surroundings and provides the basis for planning, decision-making, and control of autonomous and intelligent machines (Dong *et al.*, 2009).

Microwave data is particularly sensitive to structural content of the object. Optical data provides useful spectral information in relation to object characterisation and its penetration capabilities over complement surface view provided by microwave system. Combination of optical with microwave data can lead to an improved separation of classes within an area and can also enable identification of additional classes.

Fusion can be categorised into 3 main types: pixel based, feature based, and decision based. Fusion techniques procedure at pixel level, require that the data input registered with high accuracy of half an pixel. Feature based fusion first required that feature are identified and extracted from the separate input dataset and these extracted features are then combine to form the output. Decision based fusion requires independent classification of all input datasets. A fusion result is then generated base on the probability that each object are correctly identified in each of the separate classification (Pohl and Van Genderen, 1998).

Preparation (data selection and pre-processing) steps are crucial to the eventual result of fusion and any errors committed in the early stage will have compounding effect in all subsequent processing.

There are four levels of data fusion (Dong et al., 2009)

(1) Signal level fusion. In signal-based fusion, in which signals from different sensors are combined to create a new signal with a better signal-to noise ratio than the original signals.

(2) Pixel level fusion: Pixel-based fusion is performed on a pixel-by-pixel basis. It generates a fused image in which information associated with each pixel is determined from a set of pixels in source images to improve the performance of image processing tasks such as segmentation.

(3) Feature level fusion: Feature-based fusion at feature level requires an extraction of objects recognized in the various data sources. It requires the extraction of salient features which are depending on their environment such as pixel intensities, edges or textures. These similar features from input images are fused.

(4) Decision-level fusion: It consists of merging information at a higher level of abstraction, combines the results from multiple algorithms to yield a final fused decision. Input images are processed individually for information extraction. The obtained information is then combined applying decision rules to reinforce common interpretation.

There are several remote sensing fusion techniques that have been used in different researches such as: transformed based, statistical and numerical, filter fusion, fusion based on inter-band relations and wavelet decomposition (Vega et al., 2006) which were summarized by (Pohl and Van Genderen, 1998) and (Dong et al., 2009). In this research, two fusion techniques were IHS and Principle Component Analysis (PCA) were selected to employ.

The PCA transform converts inter-correlated multi-spectral (MS) bands into a new set of uncorrelated components. To do this approach first we must get the principle components of the MS image bands. After that, the first principle component which contains the most information of the image is substituted by the panchromatic image. Finally the inverse PC transform is done to get the new RGB (Red, Green, and Blue) bands of multi-spectral image from the principle components (Dong et al., 2009) .

IHS transformation method separates the Intensity (I), Hue (H) and Saturation (S) components of a RGB image in order to reduce dimensionality of the input data set by concentrating information into a smaller number of output channels (Abdikan et al., 2008).

To combine the information from ALOS PALSAR with optical ASTER imagery, a fusion procedure was carried out (described in Figure 4.2). First of all, an IHS fusion was used to converts the color composition of HH, HV and the ratio of HH/HV polarisation from the RGB space into the IHS color space. PCA technique was employed to combine the 9 bands of ASTER into three band namely PCA1, PCA2, PCA3. The RGB composition of these bands then was converted to IHS color space.   After that, the intensity (I) band of the optical IHS image was replaced by the intensity (I) band of the IHS radar image in the fusion to make a new IHS dataset combining all information from radar and optical image. A reverse- IHS transform is then performed on this new data set, resulting in an RGB fused image with 3 bands (after this will be known as Band A, Band B and Band C).
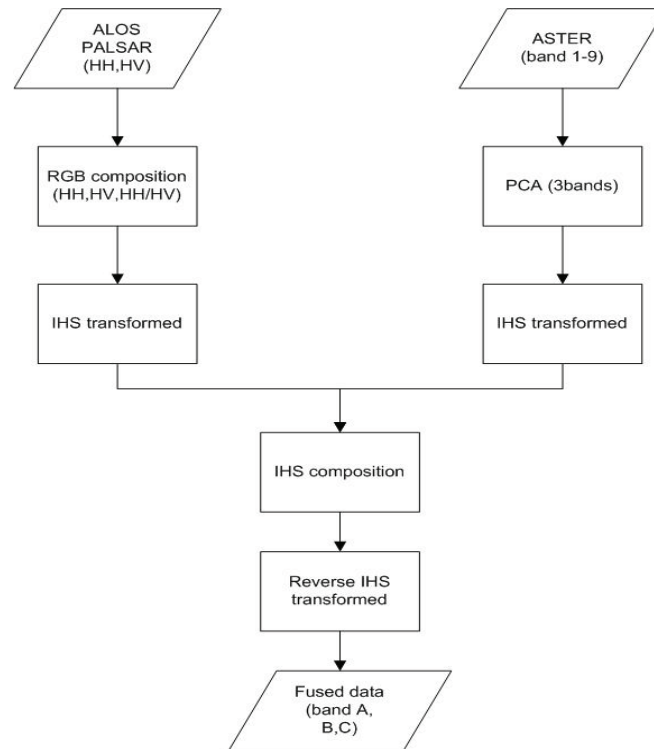
Figure 4-2 Fusion procedure of optical and radar image

4.1.4.   Image classification

The objective of classification operation is to automatically identify and categorize all pixels in an image into classes by using the analysis of multispectral image data and the application of statistically based decision rules to determine land cover identity of each pixel in the image (Lillesand *et al.*, 2004).

The supervised classification procedure consists of 3 stages (Lillesand *et al.*, 2004):
-   Training stage: to identify representative training areas and develop a numerical description of the spectral attributes of each land cover type of interest in the scene.
-   Classification stage : to categorise each pixel in image data set into the class which it most closely resembles using predefined decision rules
-   Output stage: to present the result after the entire data set has been categorised.

 The Maximum Likelihood algorithm was employed to assign each pixel to one of the four classes that has the highest probability with the assumption that they are normally distributed (Lillesand *et al.*, 2004).

The pixel based supervised classification (PBC) was used to segment the optical and radar fused image into 4 main cover types: Natural Forest, Plantation, Agro-forest, Bare ground. The classification result was validated using ground data points obtained from the field.

4.1.5.   Field work

The purpose of fieldwork phase was to measure the aboveground biomass from the study area. This data later will be used as the ground truth data for both of estimation and validation work of modelling biomass. However, in executing a forest inventory, we need to establish a relationship between directly measurable tree or stand characteristics (e.g. DBH, height) and other forest stand parameters such as volume or biomass which is impossible to be measured directly (Husch *et al.*, 2003). Therefore, the stand parameters of tropical forest will actually be measured from the field and then used for biomass calculation by allometric equations.

Pre-fieldwork

Before the trip collecting data from the field, a lot of reference data were prepared based on the available data collected about the study area (see Chapter 3). A stratified random sampling approach was applied to be followed in selecting sampling plots for the fieldwork by subdividing the forest area into subdivisions called strata on the basis of some criteria such as topographical features, forest types, density classes or volume, height, age or site classes.

The purpose of stratification is to reduce the variation with the forest subdivision and increase the precision of the population estimate (Husch *et al.*, 2003). Stratified random sampling in forest inventory has the following advantages over simple random sampling:
- Separate estimates of the means and variances can be made for each of the forest subdivisions
- For a given sampling intensity, stratification often yield more precise estimates of the forest parameters than does a simple random sample of the same size.

On the other hand, the disadvantages of stratification are that the size of each stratum must be known or at least a reasonable estimate be available and that sampling unit must be taken in each stratum if an estimate for that stratum is needed (Husch *et al.*, 2003). This can be achieved if the established strata result in a greater homogeneity of the sampling unit within a stratum than for the population as a whole (Spurr, 1952).

A land cover map was established to facilitate the stratification and ensured that samples are distributed randomly in each stratum with the number due to its size. A routine and navigation facilities were also prepared for the field trip.

Data collection from the field
A visit reconnaissance was made to bring the first impression about the study area and adjust the field schedule. After that, the data was collected in 75 plots during 3 weeks.

Different shapes of plots were used in the field base on the cover type (see Figure 4.3). The circle plot was employed in the forest and plantation with the radius 12.62 meters and only trees with DBH larger than 10 cm is measured using diameter tape. Circular plots have been used widely since the radius, a single dimension, can be use to define the perimeter (Husch *et al.*, 2003). The square plot with size 30x 30 m was employed in the agro-forestry because the trees in these plots were less dense than in the forestry and the topography was quite flat.
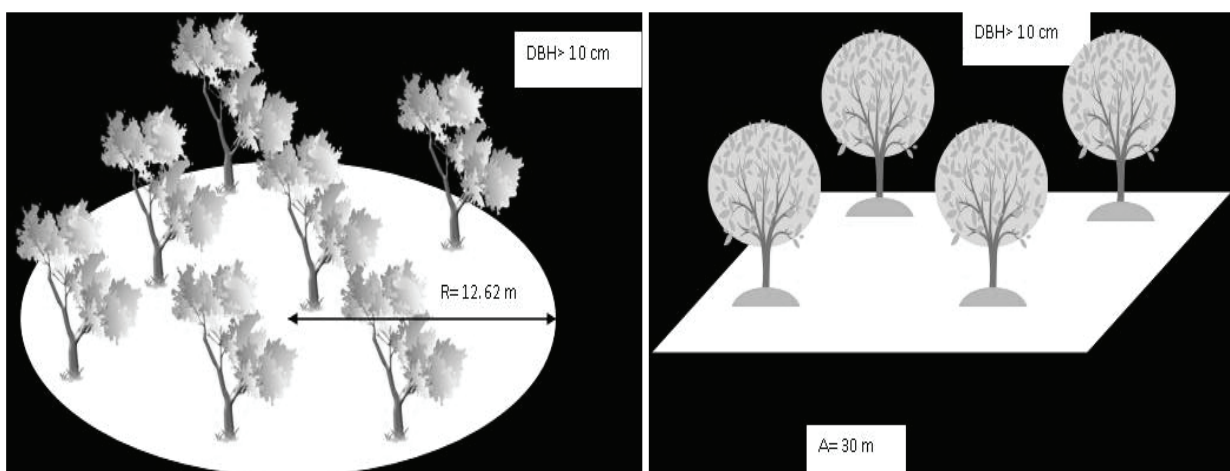
Figure 4-3 Circular plots (left) and Square plots (right)

The measurement of biophysical parameters such as DBH (cm), tree height (m), and crown cover (%) was collected. For the areas that having slope higher than 5%, the slope correction was used. Time, budget and also weather conditions were main factors that affected the field work.

Field work data analysis

Allometric equations were used to calculate the ABG biomass from volumetric or structural dimensions and most of them are based on tree diameter at breast height and tree height (IPCC 2003). Various allometric equations have been developed for tropical rain forest (Brown, 1997; Araújo *et al.*, 1999; Chambers *et al.*, 2001; Chave *et al.*, 2005; Basuki *et al.*, 2009). However, due to literature review, no allometric equation to estimate AGB biomass from bio physical parameters is available locally for Ghana.

Therefore, the following equations from IPCC 2003 were adapted to convert field data to AGB per tree.

$$Y(kg / tree) = 0.153 * DBH^{2.382} \ (a)$$

$$Y(kg / tree) = 0.2035 * DBH^{2.3196} \ (b)$$

Where Y: aboveground biomass per tree
DBH: measured tree diameter at breast height

From these equations (a) is used for Teak plantation and (b) for the others.

The AGB per tree is then summed over all the trees to obtain a stand-level AGB estimate. After that, the expansion factor is used to calculate the AGB per ha for each plot. Because of the difference in the size and shape of plots measured in different land cover types, different factors were use: 199 for circular plots and 11 for square plots.

4.1.6. Modeling above ground biomass

4.1.6.1. Correlation analysis

Correlation analysis measures the degree of association between two or more variables. Correlation expresses the joint property or relationship between two or more variables to see how closely they are associated. When correlation exists, the size of the measurements of one variable is related to the sizes of the measurements of another variable (Husch *et al.*, 2003).

The measure of the degree of association between two variables is called the correlation coefficient. It takes value between -1 and 1, where -1 indicate a perfect negative relation, +1 a perfect positive relation and the value of 0 indicates absence of relation (Stein *et al.*, 1999).

All decisions regarding the null hypothesis are based on probability, not so absolute certainty. Consequently it is necessary to indicate the probability level on which the decision to reject the null hypothesis is based. The probability is called the level of significance. Statement of significance have conventionally been given in terms not significant, significant and highly significant (Husch et al., 2003).

Table 4-1 Probabilities of Different Significance Levels (Husch *et al.*, 2003)

Significance level	Probability of Occurence	
	P	1 out of n chances
Not significant	Greater than 0.05	Greater than 1 out of 20
Significant	Less than 0.05 but not less than 0.01	Less than 1 out of 20 but not less than 1 out of 100
Highly significant	Less than 0.01	Less than 1 out of 100

In this research, correlation analysis was used to assess the correlation of biophysical parameters, AGB with radar backscatter and DN value from fusion data as shown in Figure 4-4.
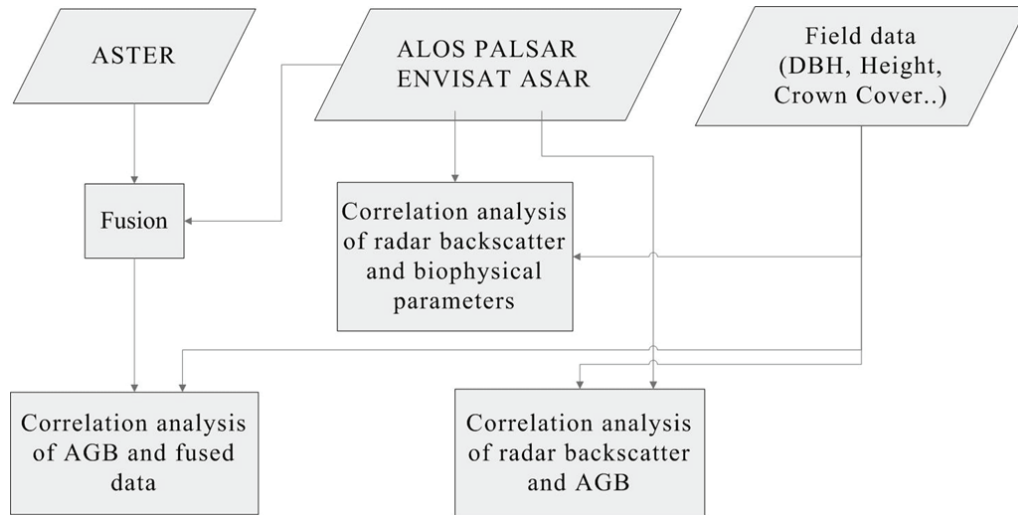
Figure 4-4 Correlation analysis approach

4.1.6.2. Geometric Sensitivity of radar backscatter data extraction from radar images

This research also is concerned about the effect of geometry to the correlation of AGB and radar backscatter. The procedure to test the sensitivity of radar geometry to correlation with AGB is described in Figure 4-5 below.
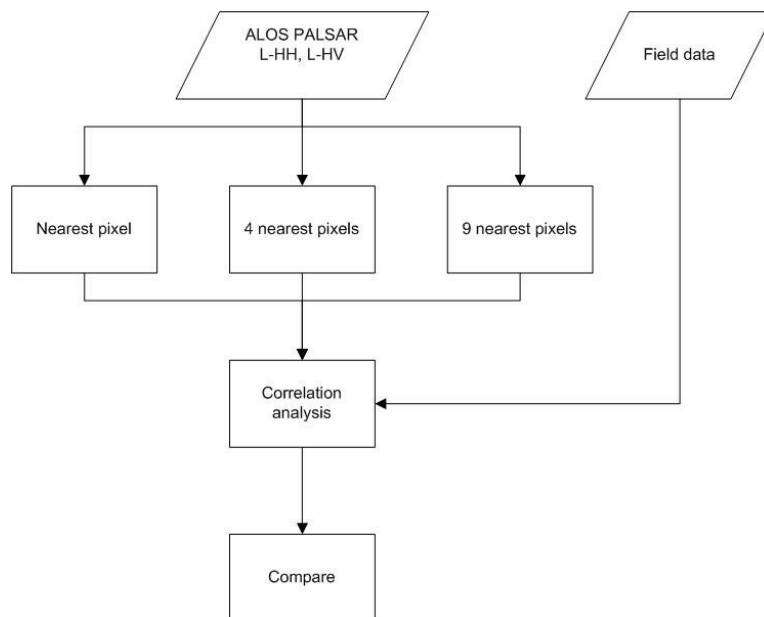
Figure 4-5 Geometric sensitive analysis of radar backcatter in relation to sampling plots location on the ground

Since the spatial resolution of ALOS PALSAR was 12.5 m, the area of 1 pixel was nearly equal to 1 circular plot measured from the field. However, it could happen that the central of the plots was not the

central of the pixel nearest to it. In that case, it was needed to consider the position of plot central on the radar image especially if the geo-referencing procedure could bring some errors to the matching between image pixels and ground sampling plots. Moreover, the GPS receiver which was used to define the location of the center of the sampling plots could also have some positioning error.

Therefore, the radar backscatter value extracted from the image was tested in 3 situations: the nearest pixel, the 4 nearest pixels and the 9 nearest pixels. Average value in each situation then was analyzed in the correlation with AGB and compared to see the geometric effect.

4.1.6.3. Regression models

The objective of regression analysis is to quantify the relationship between dependent variable and one or more independent variables. Regression implies a cause and effect relationship in which a change in the value of an independent variable will result in an expected average change in the dependent variable. The quantitative relationship is expressed by an equation and its graphic representation (Husch *et al.*, 2003). The square value of the correlation coefficient (r^2) is called the coefficient of determination. It can be interpreted as indicating the percentage of variation in one variable that is associated with other variable (Husch *et al.*, 2003).

 Regression analysis is a common way to develop AGB estimation models (Lu, 2006). After analysing the correlation of AGB and backscatter (see 4.1.6.1), it seems that single regression did not show a significant correlation. Therefore, a multi-linear regression was decided to use for modelling.

The result of previous step also indicated that not all correlations in different land cover types were strong enough for modelling (see 5.5 and 5.6). For natural forest, two input variables L band HH and HV polarised radar backscatter were chosen as an input for the multi-linear regression modelling. In plantation, the first two bands of fused image (band A and band B) were preferable to be chosen as input. No significant correlation was found in agro-forestry to model AGB in this land cover type. The AGB modelling steps for natural forest and plantation were shown in Figure 4-6.

The estimation accuracy is evaluated by using the cross validation. The dataset used to develop the multiple regression model of the relationship between backscatter of HV-HH polarisations and forest biomass is independent of the data set used to validate the model. The estimates are compared with the value observed in the field. The accuracy of result is assessed in term of RMSE and RMSE% (Holopainen *et al.*, 2009).

a)Natural forest

b)Plantation
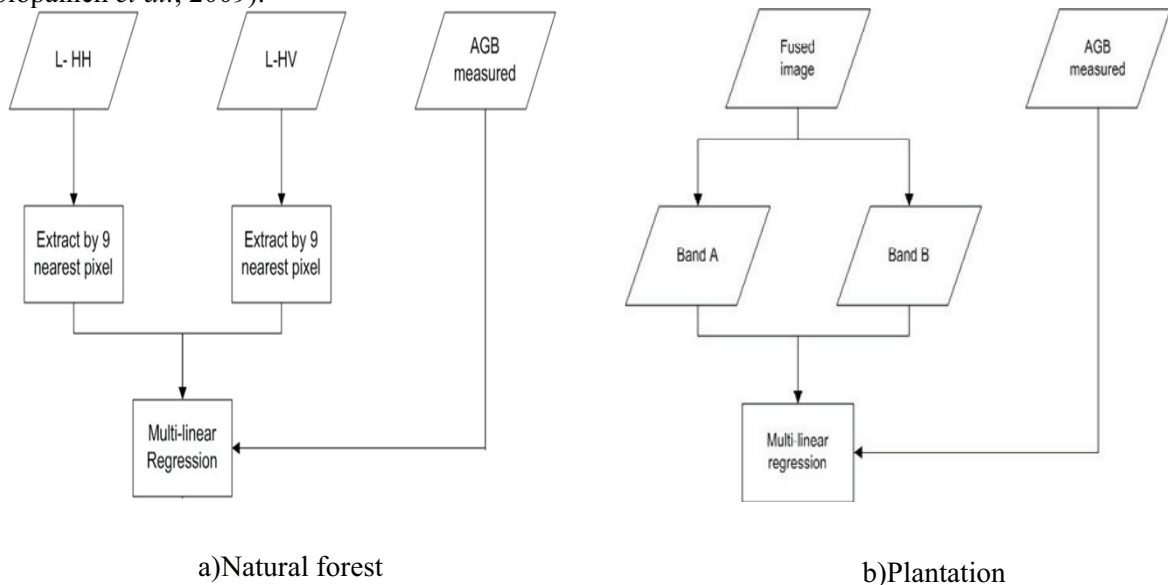
Figure 4-6 Modelling steps to estimate AGB using radar backscatter

4.1.7. Mapping biomass and carbon stock

The adjusted relation multi-linear regression equation derived above then was used to calculate the biomass and the carbon for the whole area.

The biomass value w converted to carbon stocks using a conversion factor with the equation (IPCC, 2003)

$$C = B \cdot CF$$

where C = carbon stocks (t),
B = dry biomass (t),
CF = carbon fraction of biomass (=0.5)

4.2. Material description

4.2.1. Dataset

4.2.1.1. ENVISAT ASAR data

The ASAR (Advanced Synthetic Aperture Radar) is an advanced version of the synthetic aperture radar from the ERS-1 and 2 missions. It operates at C-band (5.331 GHz) and incorporates a number of imaging modes that provide a variety of resolutions, polarisations and swath widths. Generally, the swath width is 100km with the exception of wave mode (5km) and wide swath width and global monitoring (400km) products. ASAR ensures continuity with the image mode (SAR) and the wave mode of the ERS-1/2 AMI. It features enhanced capability in terms of coverage, range of incidence angles, polarisation, and modes of operation. This is provided by significant differences in the instrument design: a full active array antenna equipped with indicated transmit/receive modules which provides distinct transmit and receive beams, a digital waveform generation for pulse "chirp" generation, a block adaptive quantisation scheme, and a ScanSAR mode of operation by beam scanning in elevation. Table 4-1 showed the technical characteristics of ENVISAT ASAR sensor (Richards and Jia, 2006).

Table 4-2 Technical characteristics of ENVISAT ASAR sensor

Technical Characteristics	
Accuracy	Radiometric resolution in range 1.5-3.5 dB
Spatial Resolution	Image, Wave and Alternating Polarisation modes: approx 30x30m
	Wide Swath mode: approx 150x150 m
	Global Monitoring mode: approx 1000x1000m
Swath Width	Image and alternating mode: up to 100km
	Wave mode: 5km
	Wide swath and global monitoring modes: 400km or more
Wave bands	C band, with choice of 5 polarisation mode (VV,HH,VV/HH,HV/HH, or VH/VV

ENVISAT ASAR used in this research was provided by ITC. This ASAR_WSM_1P mode product was acquired in March 2009 with only 1 polarisation HH that will be called as C-HH after this.

4.2.1.2. ALOS PALSAR data

ALOS (Advanced Land Observing Satellite) is designed as a follow on to JERS-1 and ADEOS (Midori). Besides PRISM (for stereoscopic mapping) and an AVINIR, ALOS carry a phased array L band SAR, to be known as PALSAR. The SAR will have a swath width of 70 km and a 2 look spatial resolution of 10m in its observation mode, and a swath width of 250-360 km with a spatial resolution of 100m in a Scansar (wide swath width) mode (Shimada *et al.*, 2009).

Table 4-3 ALOS PALSAR characteristics

Content	value
Height	691.5 km
Revolution	14-27/46 per day, 671 as total orbits
Inclination	98.16 degree
Eccentricity	0.00118
Orbital determination accuracy	Less than 40 cm
Mass	4000Kg
Solar power	7000W at the begining
Transmitter	80 TR modules for 2.0 KW
Antenna size	8.9m in azimuth and 2.9 in range
Frequency (MHz)	1270
Bandwidth (MHz)	28.0 (FSB and WB2), 14.0 (other mode)
Sampling frequency(MHz)	32.0 (FSB and WB2),16.0 (other mode)
Pulse width	27.0 (FBS,FBD,SCANSAR), 17.0 (polarimetry)
Mode	Fine Beam Single (FBS), Fine Beam Dual (FBD), Polarimetry (PLR), SCANSAR (WB1 and WB2), Direct Single (DSN)
Number of beams	18 for STRIP mode, 5 for SCANSAR
AD converters	1-Q, 5 bits
Swath width	70 km on ground (STRIP), 350 km SCANSAR
Gain control	Manual gain control (MGC) is always used for operation mode while automatic gain mode is available

The ALOS PALSAR data used for this research was acquired in January 2009 with 2 polarisation HH and HV which after this will be called as L-HH and L-HV.

It was a fine mode product with level 1.5. The features of this product type can be found in the table below:

Table 4-4 Processing parameters of level 1.5 fine mode

Map projection	UTM
Framing	Geo-reference, Geo-code
Image direction	Map
Resampling	Nearest Neighbour, Bi-linear, Cubic Convolution
Geodetic coordinate (Earth mode)	GRS80
Scene Shift	-5 to 4
Window function	Rectangle
Multi –look number	4 looks
Pixel spacing	12.5m

4.2.1.3. ASTER data

The Advanced Spaceborne Thermal Emission and Reflection Radiometer (ASTER) is an advanced multispectral imager with a high spatial, spectral and radiometric resolutions for EOS-AM1 platform that covers a wide spectral region from visible to thermal infrared by 14 spectral bands. Moreover, ASTER has a stereoscopic viewing capability by a near infrared band. Excellent observational performance can be expected by a pushbroom type visible and near infrared radiometer (VNIR subsystem) with a high spatial resolution of 15 m, a pushbroom type short wave infrared radiometer (SWIR subsystem) with a high spectral resolution and a whiskbroom type thermal infrared radiometer (TIR subsystem) with high spatial, spectral and radiometric resolutions (Fujisada, 1994).

Table 4-5 Tecchnique characteristics ((Abrams, 1999; Richards and Jia, 2006))

Technical Characteristics			
	VNIR	SWIR	TIR
Spatial resolution (m)	15	30	90
Data rate (Mps)	62	23	4
Swath widths	60	60	60
Stereo	Y	N	N
Wavelength region	Band	Band width	
VNIR	1	0.52-0.67	
	2	0.63-0.69	
	3	0.76-0.86	
SWIR	4	1.60-1.70	
	5	2.145-2.185	
	6	2.185-2.225	
	7	2.235-2.285	
	8	2.295-2.365	
	9	2.360-2.430	
TIR	10	8.125-8.475	
	11	8.457-8.825	
	12	8.925-9.275	
	13	10.25-10.95	
	14	10.95-11.65	

An ASTER image acquired in March 2008 in was selected for this study. This image was a Level 1-B product in which the radiometric and geometric calibration was carried.

4.2.1.4. Other reference dataset

Besides, there are other reference data provided by ITC that was used in this research, including:
- Topographic Map at 1:50000 scale
- Ghana geo-database (soil type, land cover, geological types, culture area etc.)

4.2.2. Other materials

In addition to the dataset, other materials were used including:
- Instruments to support for the field work (listed in Table 4-7)
- Software to support data analysis and thesis writing (listed in Table 4-8)

Table 4-6 List of instruments used for field work

Instrument	Purpose of usage
iPAQ and GPS	Navigation
Prismatic compass	Orientation
Diameter tape 5 meters	Diameter measurement
Measuring tape 30 meters	Length measurement
Spherical densiometer	Crown Cover measurement
Clinometer haga	Height Measurement
Fieldwork datasheet	Field data record

Table 4-7 List of software used in thesis

Software	Purpose of usage
ArcGIS Destop version 9.3.1	GIS analyzing
ENVY version 4.7	Remote sensing Image processing
Erdas Imagine 9.3	
R (Software package for statistical computing)	Statistical analysing
Microsoft Excel	
SPSS	
Adobe Acrobat Professional	Thesis writing and editing
Microsoft Word	
Microsoft Visio	
Microsoft Project	

5.   Results

5.1.   Landcover mapping using radar and optical fused image

Fusion data of ALOS PALSAR radar and ASTER optical image (figure 5.1) was classified into 4 main land cover types: Natural forest, plantation forest, grassland and agro-forestry using Maximum Likelihood Classification algorithm.
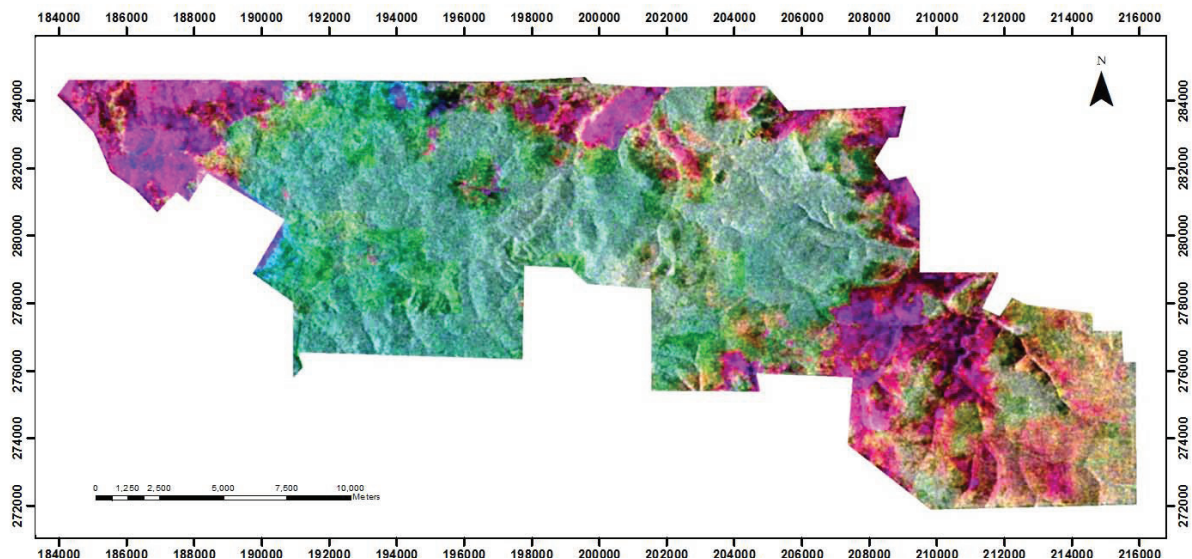
Figure 5-1 Fused image of ALOS PALSAR and ASTER

From the classification result, the area of each land cover class and the total area of the study area were calculated and presented in Table 5-1 below.

Table 5-1 Area of each class and total area in the study area

Class	Area (ha)
Grass land	315.7
Plantation forest	4605.3
Agro-forestry	10141.6
Natural forest	4835.0
Total	19897.6

The classification result was validated using 64 sampling plots (30 in agro-forestry, 17 in natural forest, 2 in grassland and 15 in plantation). From the confusion matrix of errors (see Table 5.2), the accuracy of classification was assessed based on Producer's accuracy, User's accuracy and Overall accuracy represented in Table 5.3.

Natural forest and agro-forestry were classified correctly the most with user accuracy of 87.5 % and 83.87% respectively and producer accuracy 82.35% and 86.67 % respectively. Grassland classification was less correct with 66.67% user accuracy. The overall accuracy of classification result was 81.25%. The classification result then was used to create land cover map for Afram Headwater Reserve shown in Figure 5.2 as below.

Table 5-2 Confusion matrix of errors for classification

Classification	Reference				
	Agro-forestry	Natural forest	Grassland	Plantation	Total
Agro-forestry	26	1	1	2	30
Natural forest	1	14	0	2	17
Grassland	0	0	2	0	2
Plantation	4	1	0	10	15
Total	31	16	3	14	64

Table 5-3 Accuracy assessment of classification

Class	Reference Total	Classification Total	Correct Total	Producer's Accuracy	User 's Accuracy
Agro-forestry	30	31	26	86.67%	83.87%
Natural forest	17	16	14	82.35%	87.5%
Grassland	2	3	2	100%	66.67%
Plantation	15	14	10	66.67%	71.43%
Total	64	64	52		
Overall accuracy = 81.25 %					

The major land-cover type in this area was agro-forestry which accounting for more than 50% area. The area of plantation forest and natural forest only contribute to approximately less than 25 % each. Grassland has the smallest area which was less than 5 %.
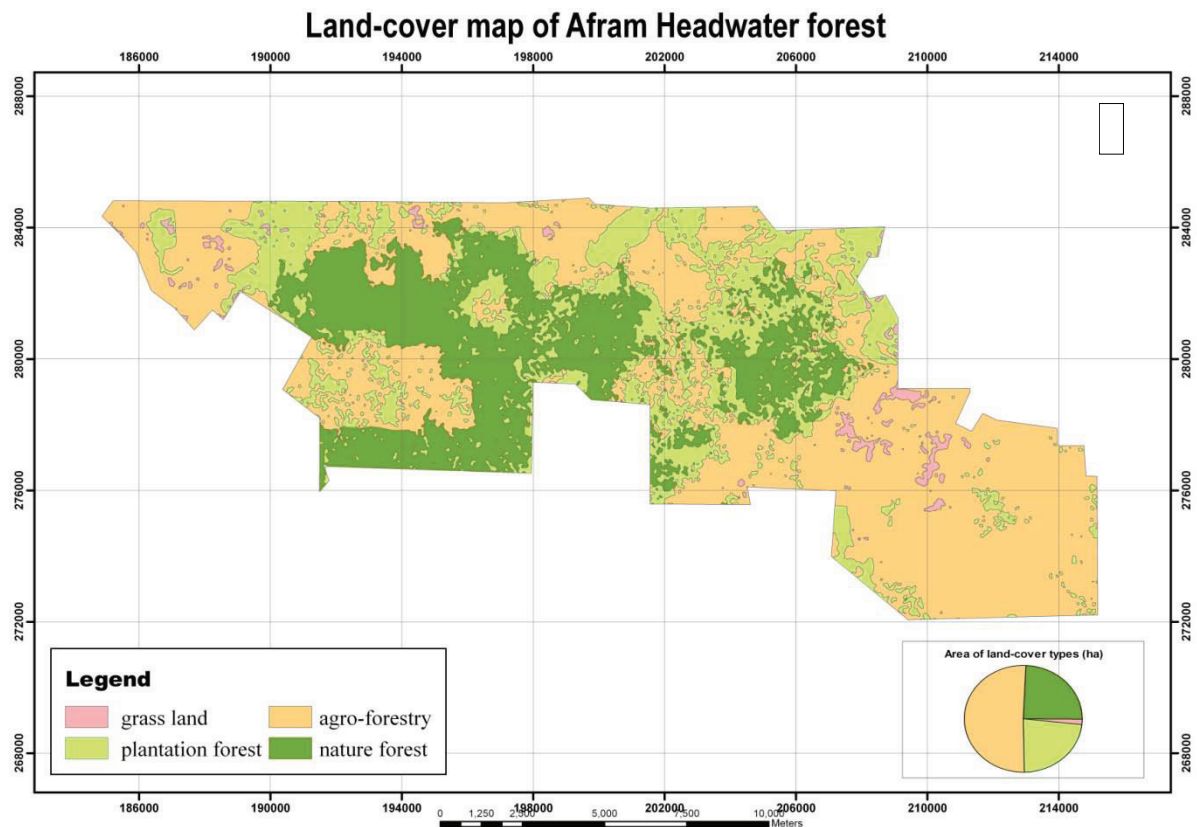
Figure 5-2 Land cover map of Afram Headwater forest

5.2.   Descriptive analysis of field data

Measurement of forest stand parameters (average DBH, number of tree, canopy height and crown cover) were analysed and presented by box-plots shown in Figure 5.3 for each cover types were forest trees are present (i.e. Natural forest, Plantation and Agro-forestry).

As can be seen, average DBH value measured in agro-forestry was the largest with the mean value approximately 50 cm and also varied the most in the three main land-cover types. However, in the crown cover measurement, natural forest and plantation forest showed a much higher result (60 -80% cover) compared to agro-forestry (less than 20%).

While the trees measured in plantation plots were the shortest (averaging 12 meter) and less variability than in agro-forestry. Tree height in agro-forestry varied from 10 to more than 30 meters, higher than in natural forest that varied from 13 to 28 meters.

a) Average DBH

b) Number of tree in each plot

c) Crown Cover

d) Tree Height
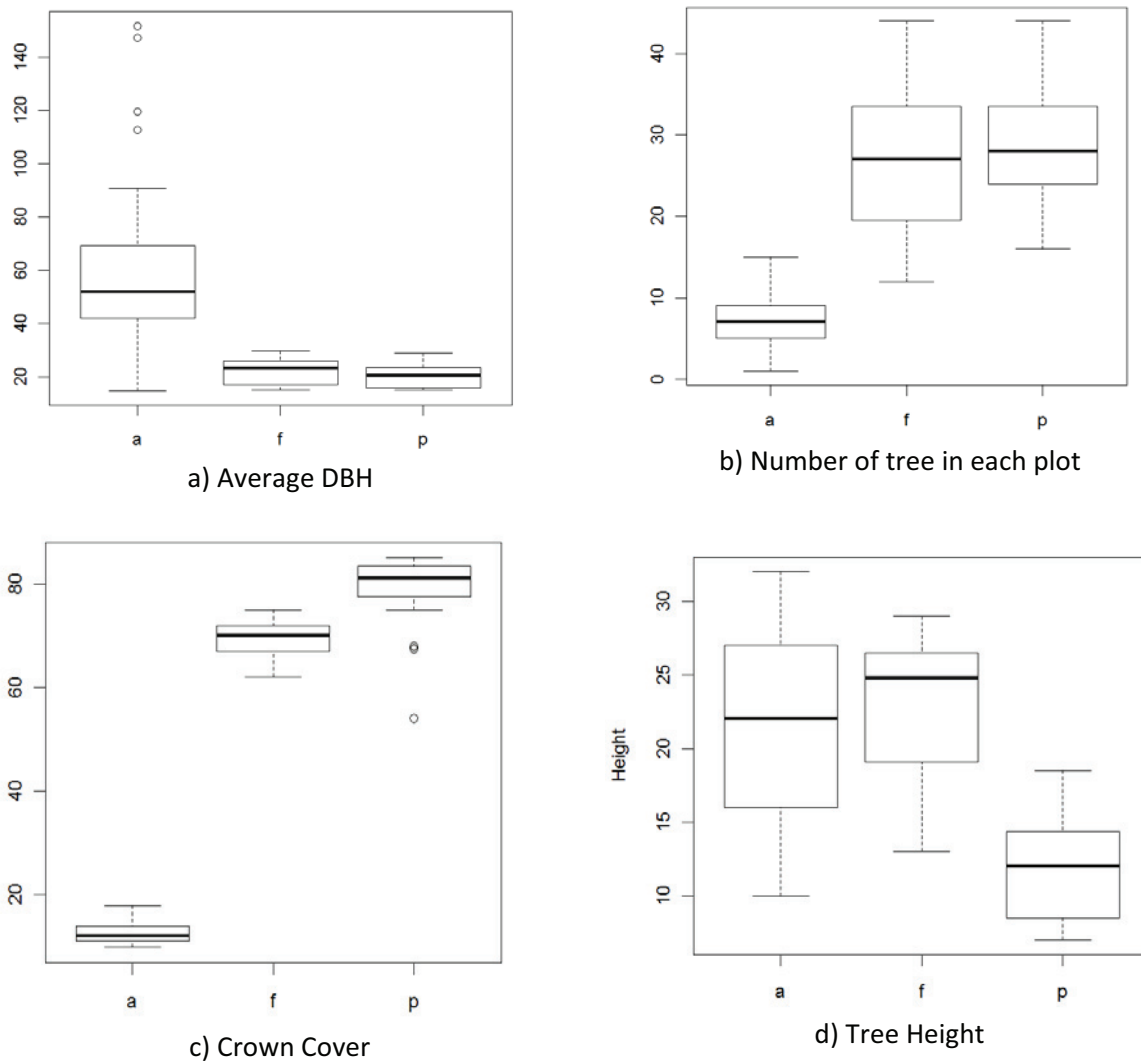
Figure 5-3 Box-plots of measured parameter in different land cover types

Agro-forestry (a), Natural forest (f), plantation forest (p)

The number of trees in natural forest and plantation plots was similar except a slight smaller in natural forest. In contrast, less than 10 trees were found in the agro-forestry plots indicating the smallest density in this land cover type.

The same trend can be found in crown cover measurement in which natural forest and plantation plots had much larger crown cover (70% and 80%) than agro-forestry plots (less than 20%).

AGB per hectare was calculated from the total AGB per tree in each plot using the expansion factor as described in chapter 4. The variation and distribution of this was shown in Figure 5.4.

It is clear from figure 5.4 that AGB in natural forest plot was the highest (average 300 ton/ha) and that in agro-forestry plot was the lowest (less than 50 ton/ha) among the three land cover types. AGB in plantation plots was around one third the amount found in Natural forest.
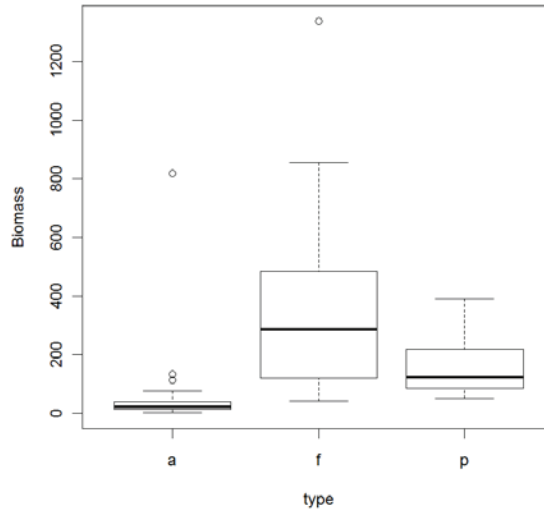
Figure 5-4 Box-plots of measured AGB in different land cover types

Agro-forestry (a), Natural forest (f), plantation forest (p)

5.3. Descriptive analysis of radar backscatter

To provide the first impression about the appearance of different land cover type (table 5-4) in available radar images, a RGB composition (as shown in Figure 5-5) was created with R= L-HH, G=L-HV and B= C-HH.

Table 5-4 Appearance of different land cover types
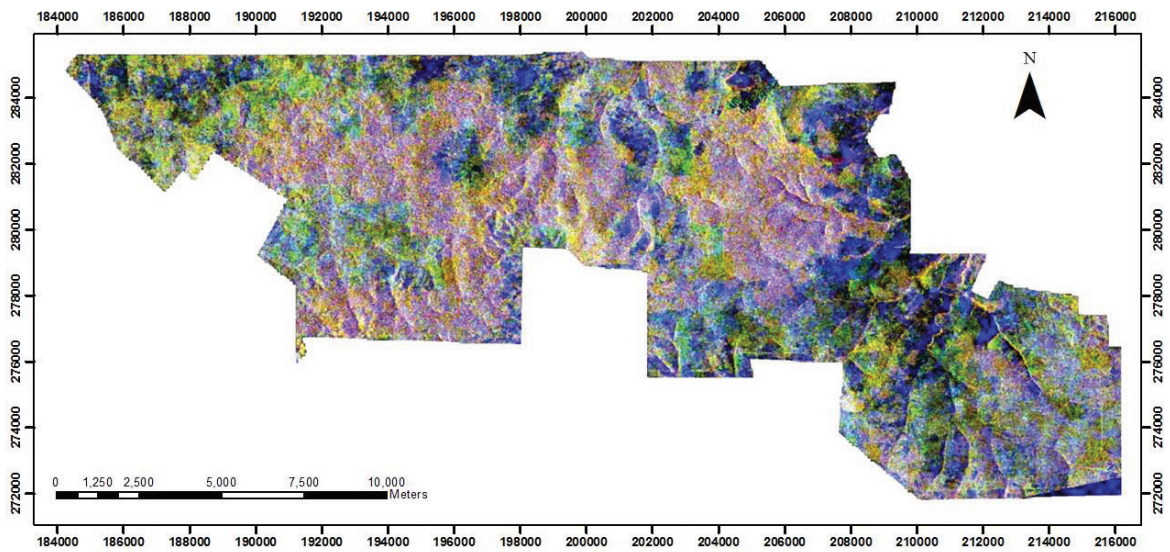
Figure 5-5 Colour composition R=L-HH, G=L-HV,B = C-HH

5.3.1. From ENVISAT ASAR

The radar backscatter value was extracted from image pixel of ENVISAT ASAR that have the same coordinates with the central point of field sampling plots. The variation of this value in different land cover type is shown using box-plots in Figure 5.6.

Similar trend in all three land cover types can be seen also in the image. Natural forest, plantation and agro-forestry were hard to be distinguished clearly from each other.
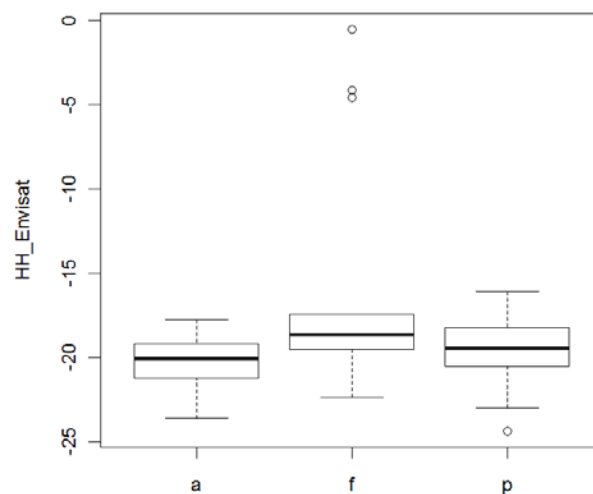
Figure 5-6 Box- plot of ENVISAT HH polarised backscatter in different land cover types

Agro -forestry (a),   Natural forest (f),   plantation forest (p)

5.3.2. From ALOS PALSAR
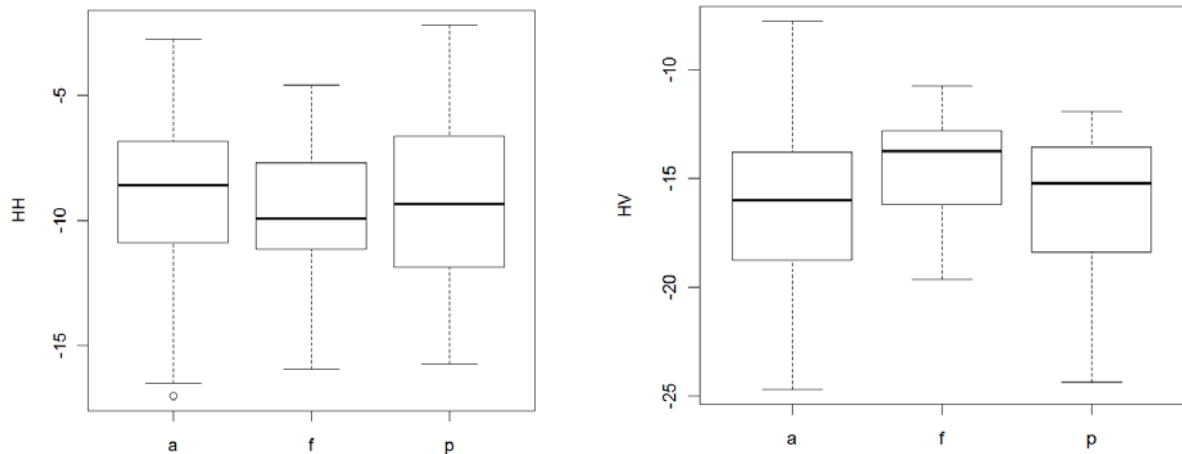
Figure 5-7 Box- plot of ALOS PALSAR backscatter in different land cover types

Agro -forestry (a),   Natural forest (f),   Plantation forest (p)

The box-plot in figure 5.7 presented the variation of backscatter value extracted from the ALOS PALSAR image. Similar to HH polarised ENVISAT ASAR, the backscatter from HH polarised ALOS PALSAR did not have much difference between land cover types. While as, box-plots of radar backscatter from HV polarised ALOS PALSAR showed distinct different between land cover types. It showed the highest scattering in natural forest, and lower in plantation and agro-forestry.

5.4. Correlation analysis of biophysical parameters and radar backscatters

5.4.1. Correlation of Canopy Height and radar backscatter

The relationship of canopy height and radar backscatter was analysed using Pearson's product-moment correlation coefficient for all plots measured from the field as shown in the Table 5.3.

Table 5-5 Pearson's product-moment correlation

	HH L band	HV L band	HH C band
t	-0.748	-1.261	0.701
df	65	65	65
p-value	0.457	0.212	0.475
95% confidence interval	-0.325	-0.381	-0.157
	0.151	0.089	0.320
Correlation coefficient	- 0.092	- 0.155	0.087

With r = -0.155 and p-value = 0.212, the relation of L band HV polarised backscatter and canopy height was significant with 75% confidence. The correlation with HH polarised backscatter either C band or L band was not significant with very low correlation coefficient (-0.092 and 0.087) and large p-value (0.4573 and 0.475).

The correlation was also analysed based on land-cover types with the results shown in Appendix D. Figure 5.8 showed a comparison of correlation coefficient of radar backscatter and canopy height stratified based on land-cover types. HV polarised L band backscatter was the highest correlated to

canopy height among the three L-band HH, L-band HV, C-band HH in all land cover types: natural forest, plantation and agro-forestry. Canopy height measured in natural forest areas showed higher correlation with radar backscatter than in other land cover types.

	L-band HH	L-band HV	C-band HH
Natural forest	0.454	0.543	0.320
Plantation	0.113	0.193	0.155
Agro-foretry	0.143	0.300	0.055
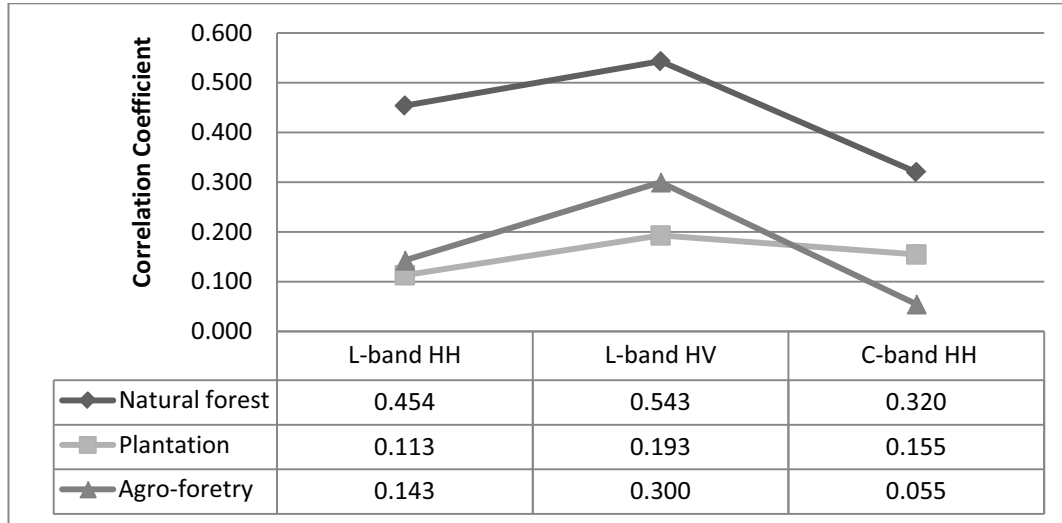
Figure 5-8 Correlation coefficient of radar backscatter and canopy height in different land cover types

5.4.2. Correlation of Average DBH and radar backscatter

The relationship of average DBH and radar backscatter for each plot was analysed using Pearson's product-moment correlation coefficient for all plots measured from the field as shown in the Table 5.4.

Table 5-6 Pearson's product-moment correlation

	HH L-band	HV L-band	HH C-band
t	0.575	-2.319	-1.277
df	65	65	65
p-value	0.567	0.024	0.206
95% confidence interval	-0.172	-0.484	-0.382
	0.306	-0.039	0.087
Correlation coefficient	0.071	-0.276	-0.156

HV polarised L band backscatter showed the highest correlation with average DBH in 95% confidence (r = -0.276 and p- value =0.023). While as, the correlation of DBH and HH polarised C band and L band was weak and not significant (r = -0.156 and 0.071; p-value = 0.206 and 0.567).

This relationship was stronger when it comes to the stratification of land-cover types as indicated in Figure 5.9. The results of correlation analysis in each land cover type were shown in Appendix D. Among those, HV L band backscatter showed a high correlation to average BDH in the natural forest with r = 0.658.

	L-band HH	L-band HV	C-band HH
Natural forest	0.045	0.658	0.207
Plantation	0.158	0.195	0.361
Agro-foretry	0.202	0.161	0.202
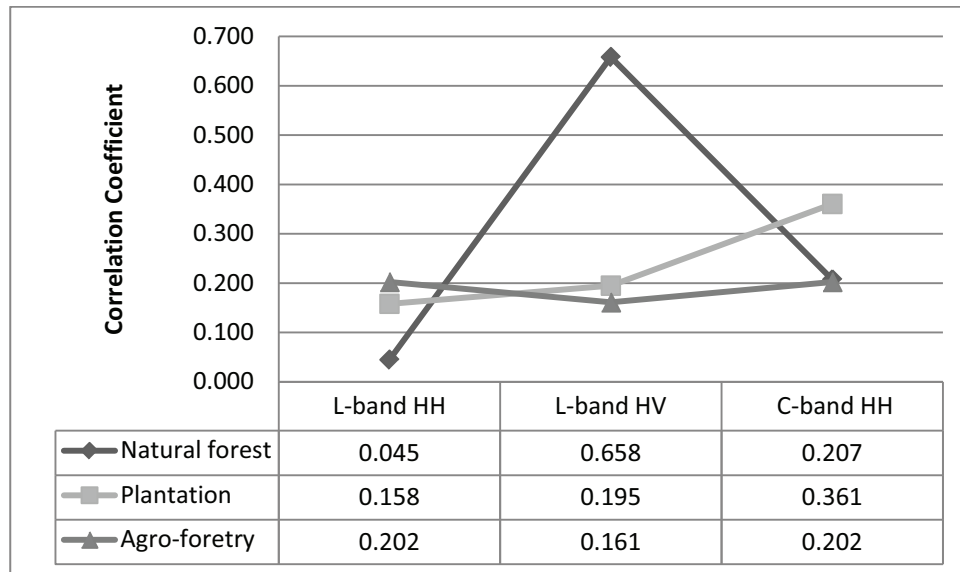
Figure 5-9 Correlation coefficient of radar backscatter and average DBH in different land cover types

5.4.3. Correlation of Crown cover percentage and radar backscatter

The relationship of crown cover percentage and radar backscatter for each plot was analysed using Pearson's product-moment correlation coefficient for all plots measured from the field as shown in the Table 5.6.

The correlation of HH polarised L-band backscatter and crown cover percentage was the strongest can be found with r = 0.3287 at 90% confidence. HV polarised L-band had the second strong and significant correlation with crown cover percentage since it had r = 0.2553 and p value = 0.030. A weak relation was of HH polarised C-band backscatter with r = 0.1591 and p-value = 0.1983.

Table 5-7 Pearson's product-moment correlation

	HH L-band	HV L-band	HH C-band
t	2.807	2.218	-1.300
df	65	65	65
p-value	0.007	0.030	0.198
95% confidence interval	0.096	0.027	-0.084
	0.527	0.475	0.385
Correlation coefficient	0.329	0.265	0.159

The correlation test was also made for each land cover type (see appendix D) and the result was shown in Figure 5.10. As can be seen, a different trend was found when HH polarised L band had the strongest correlation   in all land cover type, especially in natural forest with r = 0.526 at 95 % confidence and C band HH had the weakest and most insignificant.

	L band HH	L band HV	C band HH
Natural forest	0.527	0.324	0.014
Plantation	0.169	0.207	0.185
Agro-foretry	0.345	0.111	0.164
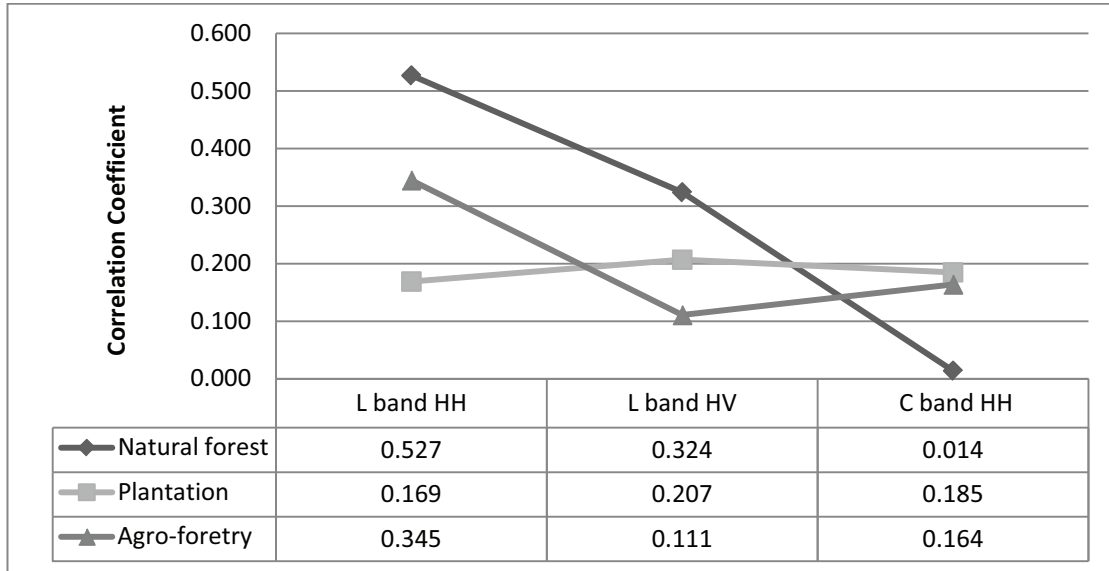
Figure 5-10 Correlation coefficient of radar backscatter and crown cover in different land cover types

5.5. Correlation analysis of above- ground biomass and radar backscatter

5.5.1. From ENVISAT

Relationship of AGB and radar backscatter extracted from ENVISAT ASAR image was examined using Pearson's product-moment correlation coefficient as shown in table 5.6 below. This relation was different in land cover types.

The strongest correlation was found in natural forest with r = - 0.310, degree of freedom df = 14 and p-value = 0.243. The relation of HH polarised C band and AGB was significant with 75 % confidence.

Table 5-8 Pearson's product-moment correlation

	Natural forest	Plantation	Agro-forestry
t	-1.220	1.159	0.936
df	14	13	36
p-value	0.243	0.267	0.356
95% confidence interval	-0.698	-0.244	-0.174
	0.219	0.707	0.452
Correlation coefficient	-0.310	0.306	0.154

Similarly, the correlation with plantation was slightly weaker with r = 0.306, degree of freedom df = 13 and p- value=0.267. The relation was significant with 70 % confidence.

The weakest correlation was in agro-forestry with r =0.154, degree of freedom df = 36 and p-value=0.356. The relation was significant with only 60 % confidence.

5.5.2. From ALOS PALSAR

The correlation of radar backscatter extracted from HH and HV polarised ALOS PALSAR image and AGB was assessed using Pearson correlation coefficient as showing in table 5.7 below. This correlation is different in each type of land cover and different polarisation.

Table 5-9 Pearson's product-moment correlation

	Natural forest		Plantation		Agro-forestry	
	HH	HV	HH	HV	HH	HV
t	-1.153	-3.451	-1.063	-0.598	1.901	1.577
df	14	14	13	13	36	36
p-value	0.270	0.004	0.307	0.5602	0.065	0.124
95% confidence interval	-0.707	-0.889	-0.694	-0.623602	-0.019	-0.071
	0.246	-0.2774	0.268	0.381	0.567	0.531
Correlation coefficient	0.305	0.691	0.283	0.164	0.302	0.254

In natural forest, HV polarised L band correlated to AGB strongly and significant with 95% confidence and r= -0.63174. The correlation of HH polarised data was weaker and significant with 70% confidence and r = -0.29425.

In plantation forest, with 65% confidence, the correlation of HH polarised data was found to be significant but very weak (r =-0.282689). No significant correlation of L band HV polarisation was found with AGB (p-value= 0.5602 and r= -0.163601)

In agro-forestry, both HH and HV polarised L band backscatter showed a positive weak correlation with AGB. The correlation of HH polarised L band was significant with 90% confidence and multiple R = 0.3020658. Weaker than that, HV polarised L band's correlation was significant with 85% confidence and r = 0.2542332.

5.6. Correlation analysis of above-ground biomass and optical and radar fused data

5.6.1. Natural forest

Correlation of AGB and pixel value extracted from 3 bands of the optical and radar fusion image was tested using Pearson correlation coefficient.

Table 5-10 Pearson's product-moment correlation

	Band A	Band B	Band C
t	1.769	-0.804	-0.787
df	13	13	13
p-value	0.100	0.436	0.445
95% confidence interval	-0.093	-0.657	-0.654
	0.777	0.332	0.336
Correlation coefficient	0.440	-0.218	-0.213

Only band A showed a significant correlation (r= 0.440) with AGB at 85% confidence. Neither band B nor band C correlated with AGB significantly (p-value = 0.436 and 0.445 respectively).

5.6.2. Plantation forest

Correlation of AGB and pixel value extracted from 3 bands of the optical and radar fusion image was tested using Pearson correlation coefficient.

Table 5-11 Pearson's product-moment correlation

	Band A	Band B	Band C
t	1.428	2.248	-0.149
df	13	13	13
p-value	0.177	0.043	0.884
95% confidence interval	-0.178	0.023	-0.542
	0.741	0.819	0.481
Correlation coefficient	0.368	0.529	-0.041

Band A and band B showed a quite high correlation with AGB with r= 0.361439 and 0.5289811, significant at 80% and 95 % confidence repetitively. There was no correlation existing between band C and AGB since the p-value of this relation was 0.8842.

5.6.3. Agro- forestry

Correlation of AGB and pixel value extracted from 3 bands of the optical and radar fusion image was tested using Pearson correlation coefficient.
As can be seen, the strongest correlation was in band A with r=-0.261 at 80% confidence. The other two, band B and band C's correlation were weak and had low level of confidence (band B - r = -0.119 and p value = 0.476, band C - r =-0.206 and p value = 0.216).

Table 5-12 Pearson's product-moment correlation

	Band A	Band B	Band C
t	-1.624	-0.721	-1.261
df	36	36	36
p-value	0.113	0.476	0.215
95% confidence interval	-0.536	-0.423	-0.493
	0.064	0.208	0.122
Correlation coefficient	-0.261	-0.119	-0.206

5.7. Modelling above-ground biomass using radar backscatter in Natural forest

5.7.1. ALOS PALSAR radar backscatter of AGB

The variation of radar backscatter from HH and HV polarised L-band image can be represented using values extracted in 9 pixels which are closest to the central point of sampling plot. Figure 5.8 showed the box-plot of these values in each plot.

The correlation analysis was employed again to see the effect of this variation to the correlation with AGB. Repetitively, the mean of 4 pixels and 9 pixels which were closest to the plot centre was calculated and analysed the correlation using Pearson correlation coefficient as in table 5.11.

Table 5-13 Pearson's product-moment correlation

	1 pixel		4 pixels		9 pixels	
	HH	HV	HH	HV	HH	HV
t	-1.153	-3.451	-3.330	-3.296	-1.798	-6.674
df	13	13	13	13	13	13
p-value	0.269	0.004	0.005	0.006	0.095	0.000
95% confidence interval	0.246	0.277	0.255	0.248	0.086	0.669
	0.707	0.889	0.884	0.882	0.780	0.960
Correlation coefficient	0.305	0.691	0.678	0.675	0.446	0.880

Extracted from HV polarised L band, strongest correlation can be found in mean of 9 closest pixels (r = 0.880 at 95 % confidence). The correlation of mean of 4 closest pixels was also significant but slightly weaker (r = 0.675 at 95 % confidence).

The opposite was true for HH polarised L band. The mean of 4 closest pixels showed a stronger correlation to AGB (r = 0.678 at 95 % confidence) than that of 9 closest pixels (r=0.446 at 70 % confidence).
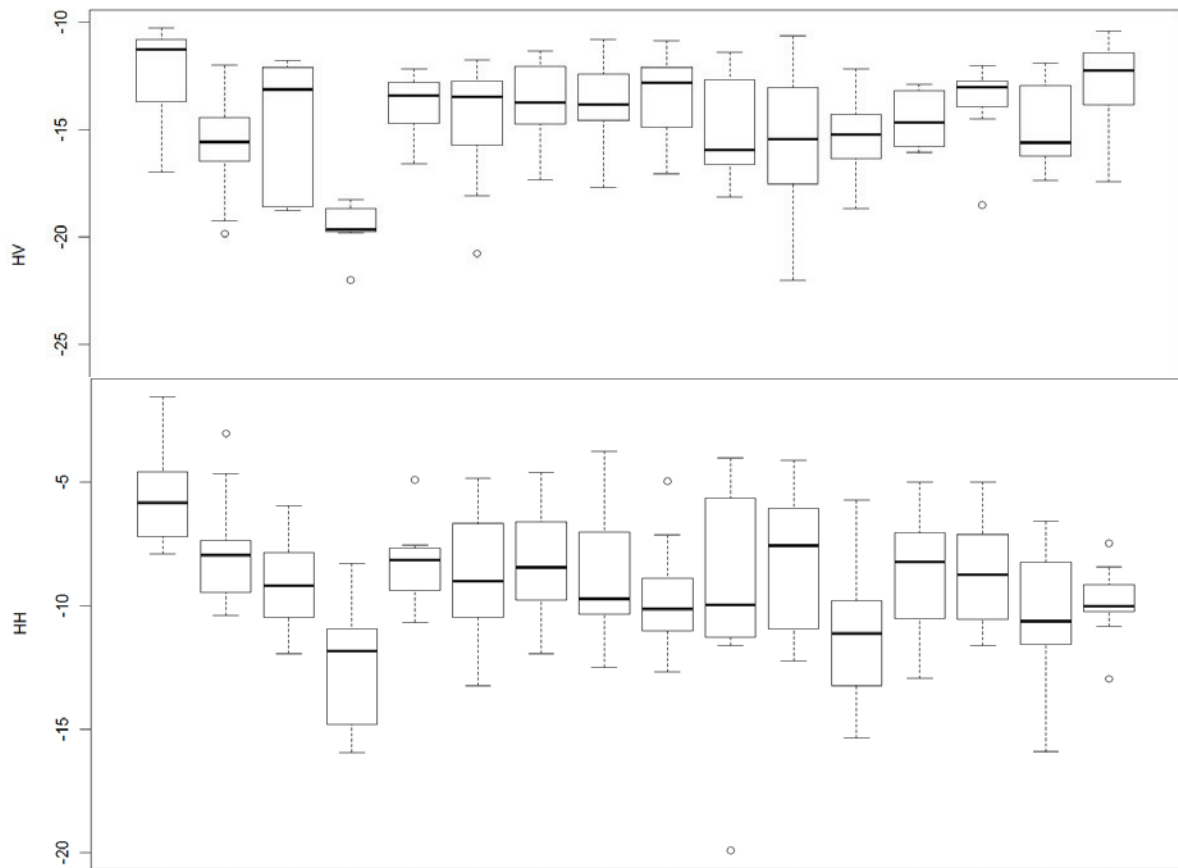
Figure 5-11 Box-plot of backscatter values extracted from 9 closest pixels in each sampling plot

5.7.2. Model adjustment

The multi –linear regression model was used to test whether a combination of multi-polarisation of HH and HV L band could bring a stronger relation with AGB. Applied for the 9 closest pixels case, the result was shown in the Table 5.13 and Table 5.14.

Table 5-14 Multi-linear regression analysis

Model		Coefficients		t	Sig.
		B	Std. Error		
1	(Constant)	2125.164	497.003	4.276	.001
	HH	-85.596	40.890	-2.093	.058
	HV	236.913	34.905	6.787	.000

The one way ANOVA test was employed to test the significance of the R^2 and the result shown in Table 5-15 indicated that the multi-linear regression was really significant.

Table 5-15 ANOVA test result

	df	SS	MS	F
Regression	2	323062.776	161531.4	30.25507
Residual	12	64067.820	5338.985	
Total	14	387130.596		

The estimated and measured AGB were plotted against each other and calculated the co-efficient of determination R^2 as presented in Figure 5-12. It was clear from the figures that the multi-linear regression model using the mean of 9 pixels extracted from HH and HV polarised L band image (with $R^2 = 0.834$) was sufficient.

The confident interval of the model was also considered with 95 % confidence. Figure 5-13 showed the variation of AGB estimated by the model.
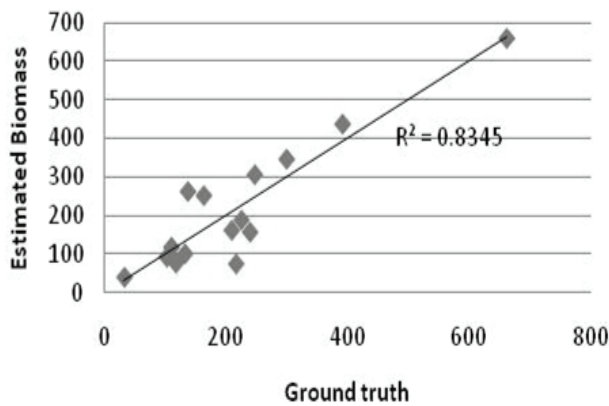
Figure 5-12 Model Adjustment Result
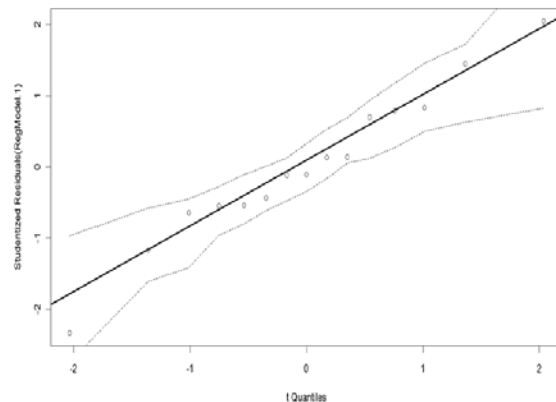
Figure 5-13 Confidence boundary of model

5.7.3. Model validation
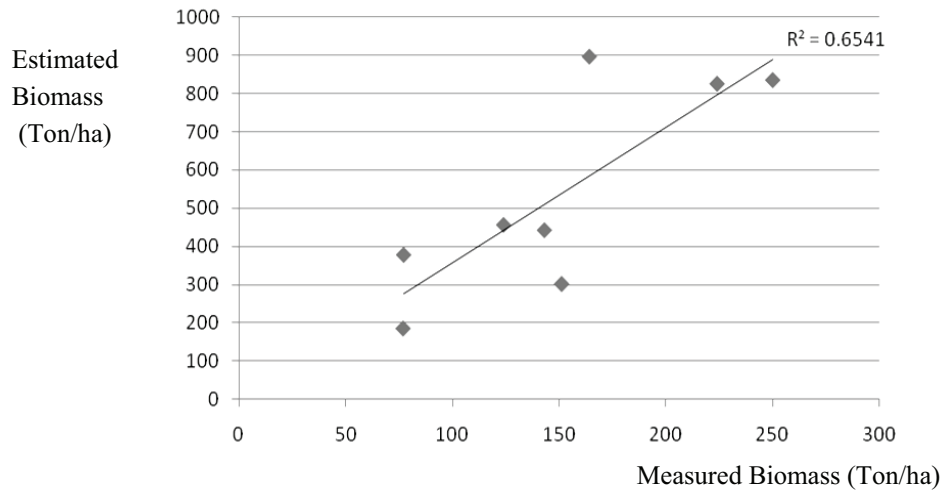
Figure 5-14 Scatter-plot graph of estimated and true value of validation plots

The multi-linear regression model was validated using 8 plots. The RMSE (root mean square error) of the value estimated by the model was quite high (179 ton/ha). The estimated value were scattered against the ground truth value obtained from the field as shown in Figure 5.10. A fit-of goodness line was added and the $R^2 = 0.65$ showed that 65% of ground truth data was explained by the estimated value using this model.

5.8. Regresion analysis in plantation

A multi-linear regression model of band A and band B from the fusion image was employed to estimate AGB in plantation forest represented in table 5.13

Table 5-16 Multi-linear regression analysis

Multiple R	0.662471483	
R Square	0.438868466	
Adjusted R Square	0.345346543	
Standard Error	4153.794246	
Observations	15	
	Coefficient	*P-value*
Intercept	9831.140425	0.152184
Band A_av9	-315.814889	0.070166
Band B_av9	357.3082502	0.025172

ANOVA

	df	*SS*	*MS*	*F*	*Significance F*
Regression	2	161935067.7	80967534	4.69268	0.031216776
Residual	12	207048079.6	17254007		
Total	14	368983147.3			

Although the relation was significant, the result estimated by this model was quite poor with $R^2 = 0.439$. However, this showed an improvement in correlation with AGB if compared to the result in plantation in previous parts.

5.9. Mapping above-ground biomass and carbon stocks in Natural forest

The multi-linear regression model of HV and HH polarised L band was decided to estimate the AGB in the Natural forest following the equation

$$Y= -85.596*X1+236.913*X2 – 2125.164$$

In which

      Y: estimated above-ground biomass (ton/ha)
      X1: backscatter value extracted from HH polarised L-band
      X2: backscatter value extracted from HV polarised L-band

The result of AGB estimation for Natural forest in the study area was shown in Figure 5.15. From the map of AGB, it can be seen that over the area the amount of AGB was mostly from 100 up to 200 ton per ha. In some parts of the area where was closed to boundary with other land cover types, this decreased to less than 100 ton per ha, especially near the boundary of the reserve, because of degradation. Only a minor area has AGB value higher than 300 ton per ha in which was far from the boundary, less degraded and difficult in accessibility.

Figure 5.16 presented the map of carbon stocks in natural forest calculated from AGB map. Because this map was made based on AGB biomass, it has a similar trend in the carbon stocks distribution. The area that has difficulties in accessibility was the largest carbon stocks with the amount higher than 150 Mg per ha. The carbon stocks with the amount less than 100 Mg per ha was found in the easy accessible area that near the boundary of the reserve and other land cove types. It account for the majority over the study area.
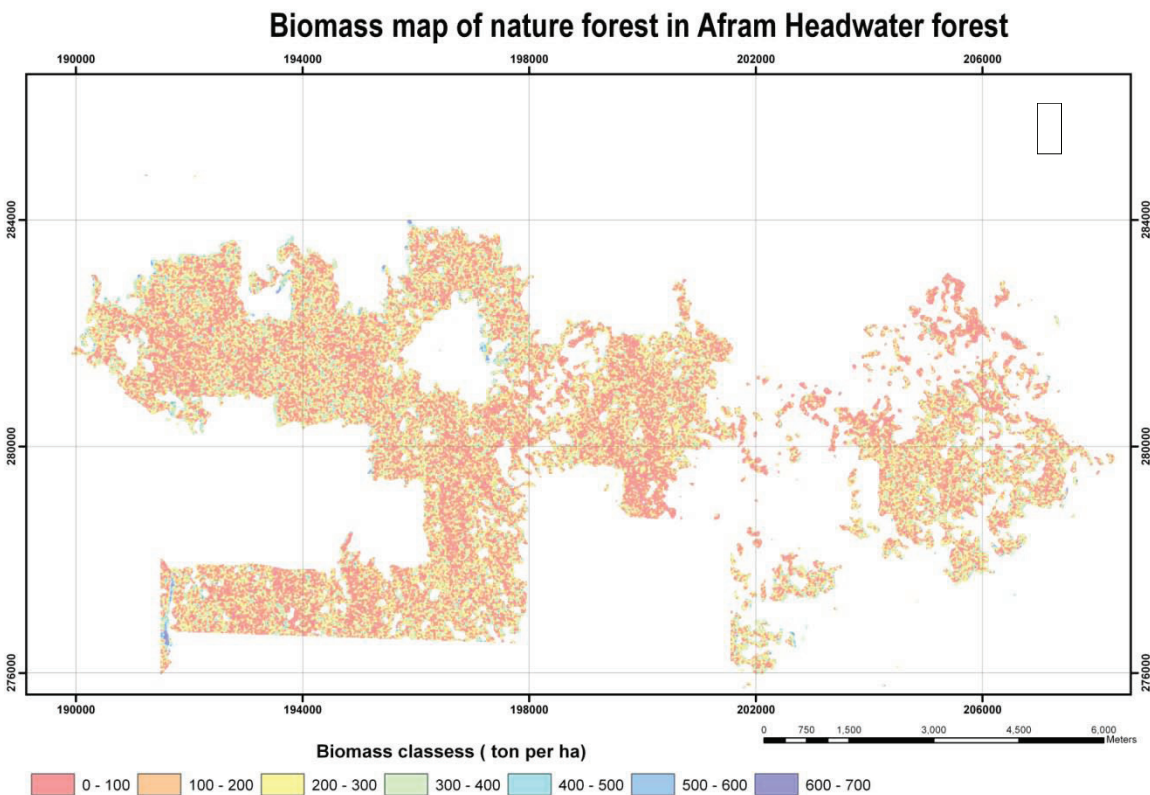
Figure 5-15 Map of estimated AGB in Natural forest
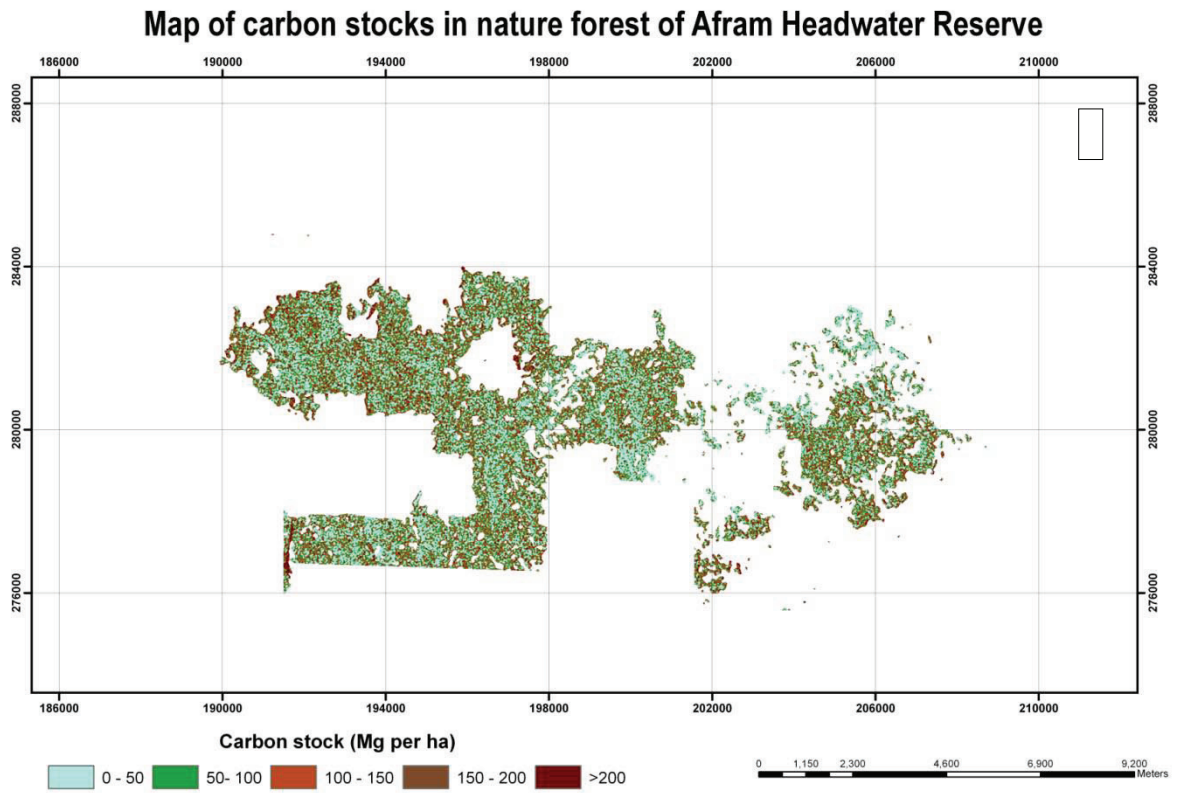
Figure 5-16 Map of estimated carbon stock in natural forest

6. Discussion

6.1. Correlation of forest stand parameters measured from the field and radar backscatter

Standing biomass of a given tree species is mainly a function of DBH, tree height and density which depends on tree age, forestry practices and also environmental and genetic factors (Kasischke and Christensen, 1990). Therefore, there must be a good relationship between radar backscatter and biophysical parameters to exploit the use of SAR backscatter to determine AGB since radar energy respond to biophysical characteristics of forest. Correlation of three radar backscatter types (C-band HH, L-band HH, L-band HV) and forest stand parameter measured from the field was analysed and the results were shown in section 5.4.

General speaking, strongest correlation was found with HV polarised L band backscatter and most biophysical parameters. Other correlations of HH polarised both L-band and C- band with stand parameters were not strong. These results are because of a deeper penetration of such long wavelength radar energy like L-band compared to short wavelength C-band and of the volume scattering from a multi-scatterer (e.g. forests) using cross polarisation.

Forest stand parameter which showed the highest correlation to radar backscatter was found for DBH with the L-band HV (r = 0.691 with 95% confidence in natural forest). Because AGB is mainly calculated from DBH using allometric equation shows strongly correlation with HV radar backscatter. This is an indication that AGB calculation using IPCC allometric equation was sufficient for this study. However, the correlation between AGB and radar backscatter was not strong in plantations and agro-forestry cover types (r = -0.283 and -0.163). An explanation for this could be that in plantation and agro-forestry, the tree density within sampling plots was not high so the backscatter was a result of surface scattering from the ground instead of volume scattering from the canopies.

The correlation of canopy height in all land cover types with L band HV was also higher (r = 0.155) compared to the other radar backscatter types C-HH, and L-HH (r =0.092 and 0.087). It can be explained by the stronger coupling of the vertical polarised wave and the vertical stalks (compared to the coupling of the horizontal polarisation wave) (Carver *et al.*, 1988). Among the three land cover types, natural forest has the strongest correlation (r = 0.543, 0.454 and 0.319) with the same reason as for DBH. Even though the correlation of canopy height was also quite strong, it was not considered as an input parameter that contributes directly to AGB estimation. The reason for this is the unavailability of local allometric equations that consider both DBH and canopy height. However, the role of this stand parameter in providing information about vegetation surface (Ustin, 2004) could not be denied.

Crown cover was the only stand parameter which has the correlation with L-band HH slightly higher than L band- HV as the result of the reflectance of like polarisation to surface scattering. This correlation was also relatively stronger in natural forest than in plantations and agro-forestry areas.

Previous research also indicated that cross polarisation is more correlated to forest stand parameters than like polarisation ((Le Toan *et al.*, 1992). In another research, (Beaudoin *et al.*, 1994) concluded that linear regression analysis between backscatter coefficients of forest stands and each forest parameter resulted in a higher correlation at HV, followed by HH and VV with general forest parameter such as stand height, DBH, tree and stand basal area (Table 6-1).

(Hussin, 1990; Hussin *et al.*, 1991) used L-band multi-polarised multiple incidence angle, aircraft SAR data to assess the correlation with forest stand parameters by comparing radar backscatter with age, DBH, basal area, height, cord per acre, tree per acre and stand biomass. The result indicated that there was a strong statistically significant relationship between HV-polarised radar backscatter and several forest stand parameters (Hussin, 1990), in particular strong positive relationship L-band HV with Slash

Pine Plantations stand parameter (Hussin *et al.*, 1991). (Le Toan *et al.*, 1992) established relationships between forest stand parameters and measurements retrieved from P-, L- and C- SAR data in which strong correlations were found with height, age, DBH and basal area at P-HV. (Leckie and Ranson, 1998) concluded that forest stand parameters and radar backscatter of long wavelength is highly correlated, such as tree age, tree height, DBH, basal area, and AGB.

Table 6-1 Correlation coefficients from linear regression analysis between radar backscatter at P and L band adapted from (Beaudoin *et al.*, 1994)

General forest parameters	*P-HH*	*P-HV*	*P-VV*	*L-HH*	*L-HV*	*L-VV*
Stand age (year)	0.72	0.73	0.49	0.57	0.53	0.46
Height (m)	0.78	0.86	0.71	0.66	0.69	0.62
DBH (cm)	0.81	0.79	0.59	0.65	0.60	0.53
Tree basal area (m2)	0.80	0.77	0.52	0.52	0.46	0.39
Tree density (per ha)	0.41	0.44	0.20	0.35	0.26	0.20
Stand basal area (m2/ha)	0.71	0.75	0.79	0.58	0.76	0.68

6.2. Correlation of above- ground biomass and radar backscatter

The relationship of AGB and radar backscatter was analysed using the method describe in Section 4.1.6 with the result shown in Section 5.6.

The correlation between AGB biomass and C- band backscatter was found to be very weak and not very significant in all type of land cover in Afram Headwater Forest. The strongest linear relationships of radar backscatter were found in natural forest and plantation significantly with only 75% and 70% confidence repetitively. In agro-forestry, a significant relationship was also identified with only 60% confidence level. The limited penetration capability of C-band was the reason for this poor correlation. Only leaves, twigs and secondary branches could be scattered with this short wavelength while the primary branches and trunk which are the major component to AGB could not be reached.

Poor relationship of radar backscatter with biomass at short wavelength was found also in several studies (Henderson and Lewis, 1998). (Pulliainen, 1996) showed that radar has low response to forest stem volume in C and X bands.(Luckman *et al.*, 1997) found out that C-band SAR system was not suitable for monitoring biomass density in regeneration tropical forest.(Hoekman *et al.*, 1996) using backscatter measurement found that the correlation between backscatter and biomass was low for C-band.

In contrast, a stronger correlation was found with backscatters at a longer wavelength (L-band) because of its capability to penetrate deeper into the canopy. Among the two polarisations of L band, HV has a stronger correlation with AGB because its vertical polarisation is a consequence of volume scattering and AGB in a way related to volume.

SAR L-band data have proven to be valuable for AGB estimation by several research from ((Wu and Sader, 1987; Dobson *et al.*, 1992; Hussin *et al.*, 1992; Le Toan *et al.*, 1992; Luckman *et al.*, 1997; Kurvonen *et al.*, 1999). HV (horizontal–vertical) polarization in longer wavelengths (L or P band) is most sensitive to biomass because it is originated mainly from the canopy volume scattering and trunk scattering(Le Toan *et al.*, 1992), and is less affected by the ground surface (Ranson and Sun, 1994; Frank Rosillo-Calle *et al.*, 2007).

Most recent research at NASA/JPL indicates that like polarised imagery shows wavelength dependent surface roughness whereas cross-polarised images present volume scattering. More specifically, L HV imagery show volume scattering from trees and dense vegetation; C-HV imagery would show volume scattering from grass and many agricultural crops and L-HH or C-HH imagery would tend to show surface scattering(Henderson and Lewis, 1998). Therefore in most cases, the operation mode with best

positive relationship with forest biomass was found to be cross polarisation at longer wave length (Henderson and Lewis, 1998).

Differences were found in the correlation between AGB and HH, HV polarised L-band backscatter value in different land cover types.

In natural forest, a strong and significant relation was found between HV polarised L-band with AGB while HH polarised L-band correlation was weaker. This also was indicated in several previous researches that are cited by (Rosillo-Calle *et al.*, 2007). (Santos *et al.*, 2003) studied the relationship of P-band SAR data with biomass values of primary forest and secondary succession of the Brazilian tropical rainforest and proved conclusively that P-band data could substantially contribute towards the development of models to monitor the biomass dynamics of tropical forests (Henderson and Lewis, 1998). (Rauste *et al.*, 1992) found that use of L-band would be limited to condition of lower biomass. Negative relations or a decrease in radar backscatter after biomass reaches higher level have also been observed (Rauste *et al.*, 1992; Ranson and Sun, 1994).

In plantation forest, the correlation of HH polarised L-band in this land cover type was similar to that found and explained in natural forest. But the insignificant relation found in HV polarised L band was different from previous research from (Wu and Sader, 1987; Hussin *et al.*, 1991; Castel *et al.*, 2002). The reason for this can be explained by the difference in management and age of plantation measured from the field in this research. These plantations show high variance in age, density, etc. In the west part of the area, the plantations were old and abandoned until the next harvest season. But in the Northeast, there were young plantations with age from 8-10 years.

As for agro-forestry, a positive relation was identified in both HH and HV polarised L band data. But HH polarisation correlated stronger than HV polarisation. In this cover type, crop and grass were dominant and trees density was very low and as a result, most backscatter was directly from the ground. Or in other word, the scattering here is surface scattering not volume scattering which related to AGB.

6.3. Factors affecting correlation of AGB and radar backscatter

6.3.1. Wavelength and polarisation

The backscatter interaction within a forest canopy includes (Henderson and Lewis, 1998):
- crown scattering
- direct backscatter from the trunks
- direct backscatter from the ground
- crown – ground backscatter
- trunk – ground backscatter.

The radar backscatter dependency on biomass varies as a function of radar wavelength and polarisation (Kasischke *et al.*, 1997). The forest structural-physiognomic characteristics and the radar's volume scattering and double bounce scattering are two important factors affecting these relationships (Santos *et al.*, 2002).

6.3.1.1. Wavelength

SAR images at varying wavelengths have different interactions with the various tree components. The wavelength will determine whether the SAR backscatter is dominated by surface scattering or volume scattering. Figure 6-1 showed the penetration of multi-frequency radar system through vegetation canopy.

When relatively short-wavelength microwave energy interacts with the surface of the forest canopy, the energy is scattered by the small-scale components of the canopy (foliage and small branches). Therefore, at these wavelengths the RADAR energy reflects mainly from the surface of the canopy.

Such a short wavelength as X-band or C-band would interact strongly with the surface of the canopy and probably penetrate the canopy surface someway to provide progressively weaker responses from the lower layers it encounters.
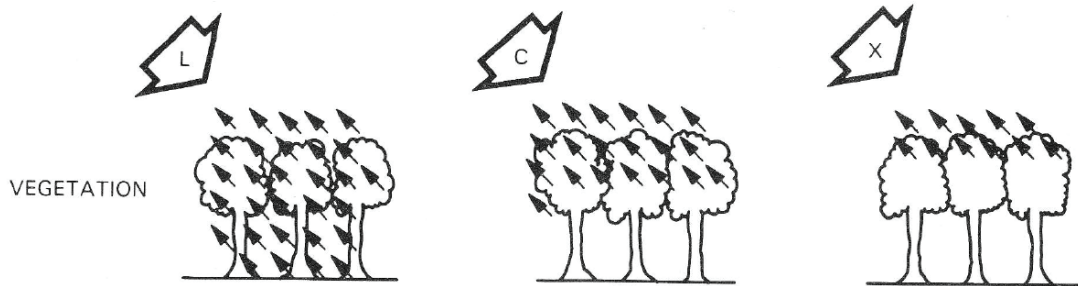
Figure 6-1 Penetration of multi-frequency radar system through vegetation (Carver *et al.*, 1988)

In contrast, radar energy with relatively long wavelengths will penetrate into the canopy and reflect from large scale components composing the canopy (large branches, stems), and the terrain surface. The reflectance is dominated by volume scattering from large-scale canopy features and surface scattering from the terrain surface (Andersen *et al.*, 2006). Longer wavelength (L- and P-band) would be likely to be interacted only weakly with the surface and upper layers of the canopy as they lack structures of sufficient size to impede the wave as it passes through. In this case the incident wave would interact most strongly with structures lower down the canopy (branches and trunk, and possibly the ground as well) but there would also be some weak contribution from the upper layer as these have to passed through twice before a signal is registered back at the receiving antenna.

The general relationship of wavelength and scattering behaviour of components in close forest was summarised by (Van de Sanden, 1997; Van der Sanden, 1997) and shown in Table 6.2 as follow.

Table 6-2 Summary of general relationship between wavelength and the scattering behaviour of the component in close forest (Van der Sanden, 1997)

Wavelength	Forest component					
	Leaves	Twigs	Secondary branches	Primary branches	Trunks	Soil
X band	++	++	++			
C band	++	+	++			
L band	-	-	++	++	++	+
P band	-	-	-	++	++	++

Notes: the mark as follows: ++ main backscattering sources, + secondary backscattering source and – attenuating source.

The longer wavelength has a high relationship to biomass and other forest stand parameters than short wavelengths (Henderson and Lewis, 1998).

6.3.1.2. Polarisation

The polarisation of incident microwave affects their interaction with forest because it defines the plane in which micro wave interaction will take place (Van der Sanden, 1997). Considering forest as a collection of vertical cylinders over a smooth surface, on their way into the forest, both horizontally and vertically polarised waves will be attenuated by the cylinders. However, due to the backscattering the loss of power for vertically polarised waves will be considerably higher than for horizontally polarised waves. Therefore, waves with a horizontal polarization will penetrate deeper than waves with a vertical polarisation. Microwaves that interact with forests and other types of vegetation are

known to become depolarized to a high degree which is caused by the multiple reflection of wave at resonant scatters, i.e. leaves, twigs and branches. Strong depolarisation implies that the backscatter wave will have a large un-polarised component. This large un-polarised component, in turn, gives rise to a substantial amount of cross polarisation which is characteristic for the vegetation. Because of its dispersing effect on polarisation, the multiple reflection interaction process in vegetation volume is often referred as diffuse scattering at surface (diffusion of polarisation) (Van der Sanden, 1997). Figure 6-2 showed the surface and volume scattering from vegetation.

Scattering from canopy top

Volume scattering

Surface scattering
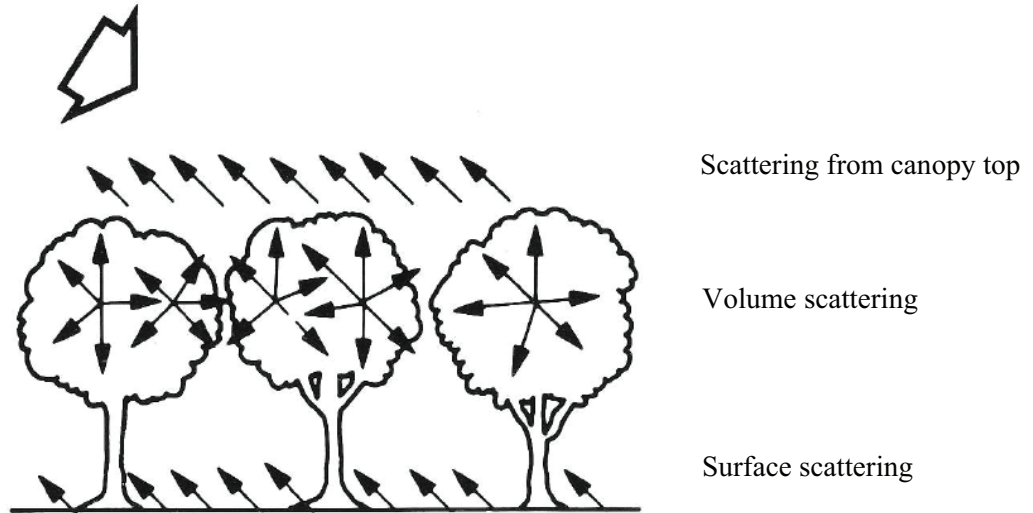
Figure 6-2 Surface and volume scattering expected from vegetated surface (Carver *et al.*, 1988)

Because radar energy can be depolarized upon interaction with various surface features, independently recording the reflection of like-polarized energy and cross-polarized energy can yield valuable information regarding the characteristics of imaged features, and can be particularly useful in the analysis of vegetation type and structure (Andersen *et al.*, 2006). If the radar energy interacts mainly with single scatterers at the surface of the canopy, the energy is not depolarized and there is a strong reflection of like-polarized energy. In contrast, if the radar energy is reflected from multiple scatterers within the canopy structure, it is often depolarized and there is a strong reflection of cross-polarized energy (Jensen, 2000). A radar image acquired from a system with a particular frequency, polarization, and incidence angle can therefore provide information related to canopy water content, vegetation type, biomass components (foliage, branches, stems), and canopy structure (Andersen *et al.*, 2006).

The three polarisation (HH, HV and VV) provide three different view of canopy structure because the wave propagation through and back scattering from the vertical stems of the plant and the trunks of the trees are polarisation –dependent. The difference between HH and VV, the later polarisation generally is more sensitive to the stalk of the plants and to the trunk of the tree because of their vertical orientation. Because of the stronger coupling of the V polarised wave and the vertical stalks (compared to the coupling of the H polarisation wave), its velocity of propagation in the canopy is slower than it is for the H signal (Carver *et al.*, 1988).

Cross-polarisation data have been found to be better than like-polarised for estimating biomass because cross polarisation is mostly due to volume scattering from the crown (Henderson and Lewis, 1998).

6.3.2. Vegetation structure

Vegetation structure and soil surface are main factors affecting the correlation with radar backscatter and caused saturation in the high biomass range (Hoekman et al 1996) like tropical forests. Structural variation might have a substantial effect on P, C, L band quad-polarisation backscatter of forest stand with equal biomass (Imhoff 1995). Precision of radar increase if structure differences between forest types are accounted for during the inversion of radar (Rignot et al 1995).

6.3.3. Other factors

Tree density will be a major consideration in determining the degree of contributions from surface and underlying vegetation. The greater the tree density and homogeneity of ground cover the more it can be sure that the backscatter is derived uniquely from one particular type of cover. However as this density reduced the greater the mixture is likely to be with contributions coming from upper, intermediate and lower layers with an additional possibility that there be some sub-surface contribution as well.

The magnitude of radar backscatter (i.e. return) from a feature is also dependent upon a variety of surface characteristics, including structure, surface roughness, and moisture content (Andersen *et al.*, 2006). Therefore they could also be factors that affect to the correlation of radar backscatter and AGB. Increasing the moisture increase the amount of interaction that takes place and as a consequence of the penetration depth reduced from that of the dry condition state. However, since the radar images were acquired during the dry season and the study area was quite flat, they are considered in this research to have no effect.

6.4. Correlation of above-ground biomass and optical and radar fused data

Optical data has been used to estimate AGB in several studies (see Section 2.1) and most of them indicated the quick saturation as the limitation of this data especially in areas with high range of biomass like in tropical forest. Some research tried to combine optical and radar data to estimate AGB but most of them were concerned only with its ability to enhance classification rather than a quantitative approach. Therefore, in this research, an effort was made to assess the correlation of fusion of radar and backscatter with AGB. The fusion approach and correlation analysis was described in Section 4.1.3 and 4.1.6 and the result was shown in Section 5.6.

In general, the correlation found in all land cover types between AGB and pixel value extracted from fusion image was weak and in some case, not significant. As mentioned above, the optical part in the fused data with radar was saturated quickly and, therefore, not corrected strongly with AGB. In the radar part of the fused data including the HH and HV polarisation L- band, only the L-band HV has really strong correlation with AGB as described in previous sections. From the fusion approach, it can be seen that this only part was then combined with other parts which do not have strong correlation to AGB and separate to three bands (band A, band B, and band C). As a result, the correlation was not improved but decreased.

The only exception was in plantation forest in which band A and band B showed a significant and relatively strong correlation with AGB. The explanation for this is the homogenous structure of canopy in plantation areas. The fused data of optical and radar was the combination of all information collected in both types of image which were compressed in 3 bands of the fused data. The first two bands are considered to contain the most information of the three. Therefore, they will have the strongest correlation among the three. In addition, the fused data is also more capable to distinguish cover types in different management and vegetation structure. It means that for natural forest, with the variation in vegetation types and canopy structure, it will be less homogenous than plantation areas which mostly are monoculture of teak plantation. Consequently, for plantation, the correlation with AGB is enhanced and become stronger. In other words, this promised a potential to estimate AGB using fusion of optical and radar data.

6.5. Geometric Sensitivity to correlation of radar backscatter with AGB

Geometry of radar backscatter was also considered as a source of error in this research since the positioning of plot center using GPS instrument and the radar calibration still contain some error that could become larger when matching the center of the plot with the pixel in the image for extractting radar backscatter. Therefore, in order to test whether it had influence on the correlation of radar backscatter and AGB, comparisons of correlation analysis between average values of one, four and

nine pixels nearest to plot central were made and it indicated effect of geometry to the correlation with AGB.

From the results in Section 5.7.1, the stronger correlation found when using the average value of 9 pixels closest to the sampling plots centre in HV L band. Even though this of HH L band was quite high, the result also showed that for HH L band, an average value of 4 pixels was slightly higher. It could be explained that the like polarisation has a stronger return than the cross polarisation when the polarisation of the transmitted microwave radiation is parallel to the domain plane of linear features. This means that the like polarised image will be generated with a higher signal to noise ratio (S/N) and therefore, will be sharper and less grainy than the cross polarised image (Henderson and Lewis, 1998).

This result indicated that the correlation of AGB is sensitive to geometry and in order to reduce this effect, it is better if the average value of 9 pixels nearest to the center of the plots was used for modelling and estimate AGB instead of using only the value the nearest pixel.

6.6. Estimating and mapping AGB and carbon stocks in tropical forest

Multiple channel radar imagery or multiple step approaches allow for estimating biomass with higher accuracy than relying on correlation between total biomass and radar backscatter from a single frequency/ polarisation ((Ranson and Sun, 1994; Dobson *et al.*, 1995; Harrell *et al.*, 1997), reviewed by (Kasischke *et al.*, 1997). The complexity of these methods is higher and the uncertainties are greater in landscapes where there are a number of different forest ecosystems with multiple tree species. Therefore, there is a need to stratify or classify the land surface containing the forest into different cover categories (Kasischke *et al.*, 1997).

6.6.1. Natural forest

The correlation of radar backscatter and AGB found in this type of land cover prove that L band HV was the most suitable input for modelling AGB in the study area. Since the L band HH also had a quite strong correlation with AGB, it was chosen together with L band HV for multi-linear regression analysis as described in Section 4.1.6. The result was shown in Section 5.7.2 concluded that the multi-linear regression model of HH and HV polarised L band was the best fit used to estimate AGB.

Validation result (presented in Section 5.7.3) answered the question about the goodness-of-fit of this model which can explain 65% the ground data. Even though the RMSE was quite high, it could be understood since the developed model was only using 15 plots and validated using 8 plots. If larger dataset had been used, the error and fitness of this model would have been improved.

The multi-linear model then was used to estimate the AGB and carbon stocks in natural forest areas in the study area. Maps of AGB and carbon stock were established and showed in Section 5.9. Over the natural forest areas, the amount of AGB was mostly from 100 to 200 ton per ha. The carbon stocks with the amount less than 100 Mg per ha accounts for the majority. It also can be seen from the maps that areas which are less degraded and difficult in accessibility have higher amount in AGB and carbon. The areas where are closed to the boundary of the reserve and other land cover types have low amount of AGB and carbon.

6.6.2. Plantation forest

Previous discussion on correlation analysis of AGB with radar backscatters and fused data of optical and radar in plantations (Section 6.2 and 6.4) indicated that the poor results were found in most cases. A gap in management status of sampling plots obtained from the field was one of the main causes for this. It would be improved if the sampling plots could be stratified base on the different managements. However, this could not be done due to the limitation of number of plots obtained from plantation. In

addition, there was not much variation in the AGB of plantation that also can be another issue for modelling.

The fusion data of optical and radar has a stronger correlation to AGB, especially band A and band B. Therefore, the multi-linear regression analysis was also done for these two bands to find out whether they can be used to estimate AGB. The method and results of this work were shown in Section 4.1.6 and Section 5.8. But this model only explained less than 50% of the estimated result. Therefore it could not be used to estimate AGB in plantation cover. However, it was indicated that this model has the potential to map plantation forest better than using only radar data. However, more field data need to be added and differentiate in management should be considered for AGB modelling.

6.6.3. Agro-forestry

No strong correlation was found in this type of land cover even using radar or the fusion or radar and optical image. Therefore, no model was developed to estimate AGB in this area of Agro-forestry. Further research and additional measurement of biomass from crops and herbal are necessary to develop a model for biomass estimation.

6.7. Uncertainty of research

Despite the large number of studies, the actual levels of uncertainty or errors in SAR biomass algorithm are not well documented. Most studies are using the standard error of the regression equation as a measure of uncertainty. This approach yields errors in the order of 10 to 20 tons/ha not an unreasonable level. However, (Harrell *et al.*, 1997) research showed that the uncertainty was two to three times the standard error of regression equation used to estimate biomass in the range of 50 to 80 ton/ha (Ustin, 2004). The uncertainties are greater in landscape where there are a number of different forest eco-systems with multiple tree species than in forest where is dominated by single tree species (Kasischke *et al.*, 1997).

There is a need to calibrate radar imagery using ground base techniques to quantify the pattern of biomass distribution in the forests of interest using valid sampling approach (Kasischke *et al.*, 1994) and stratify or classify the land surface containing the forest under study into different cover categories prior to application of the radar- based biomass estimation algorithms.

Radar saturation is also a limitation of this research. The sensitivity of radar backscatter at a single polarisation/ frequency to variation in biomass saturates after a certain biomass level is reached. The saturation point is higher for longer wavelengths and HV polarisation is the most sensitive while VV the least (Kasischke et al., 1997).

The saturation of SAR response to forest biomass is considered a distinct limitation to the usefulness of C-,L-, and P band SAR data. This poses a particular problem in tropical forest environments where AGB level generally exceed 200 – 250 Mg/ha (Ustin, 2004).

The strategy to convert forest plot data into regional – scale AGB estimation in this research also mentioned in other previous research (Brown *et al.*, 1989; Brown, 1997; Houghton *et al.*, 2001). These steps integrated a variety of technique that all contain some uncertainty as describing in Figure 6-3. (Chave *et al.*, 2004) provide a summary of the source of error in AGB estimation of a tropical forest including: tree level error, allometric model, within plot uncertainty, among plot uncertainty. The first type of error refers to the AGB estimation in s single tree. The second one related to the choice of allometric model. The last two types are sampling error which can be minimized by large sized, multi-plot, censuses.
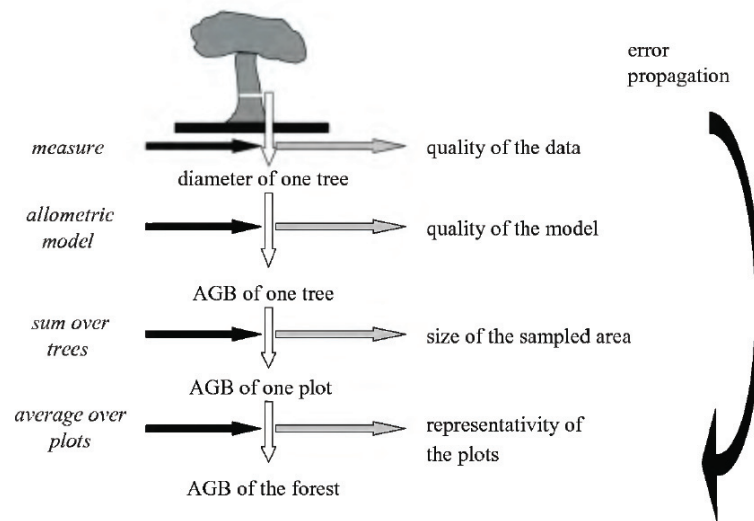
Figure 6-3 The error propagation for estimate AGB of a tropical forest from permanent sampling plots (Chave *et al.*, 2004)

AGB for individual tree was calculated using allometric equation from IPCC which, following (Basuki *et al.*, 2009), overestimated the biomass. (Cairns *et al.*, 2003) (Nelson *et al.*, 1999) also indicated the application of the site specific equation must be considered. In contrast, (Chave *et al.*, 2005) and (Gibbs *et al.*, 2007) stated that for tropical forest, generalized allometric equations must be employed because the allometric equation for local conditions or species-specific allometric equation will not improve accuracy significantly. (Ketterings *et al.*, 2001) consider the estimation error introduced in choosing a suitable functional value for any adjustment parameter in allometric equation relative to other source of uncertainty and suggest to reduce it by using average wood density as a site specific – parameter that can explain the part of variation in the model and should be include as a calibration variable where cutting and weighting of the trees is not possible for obtain a site –specific equation.
Uncertainty due to measurement errors, transect size, fraction of the above-ground biomass considered and site selection discussed by (Brown *et al.*, 1995) indicated that the dominant contributors to biomass - emergent and large canopy trees should be the focus of attention.

7.   Conclusion and Recommendation

The objective of this research is to estimate and map Above Ground Biomass (AGB) and carbon stocks for tropical forest using SAR data. To achieve this, correlation analysis was used to assess the relation of AGB and other stand parameter measured from the field with radar backscatter extracted from L- band HH and HV polarisation, C-band HH polarisation and fused data of radar and optical image. After that, a multi linear regression model was established with the chosen inputs from previous correlation analysis to estimate AGB.

Through this approach, the research questions defined in Section 1.5 were properly answered.

How strong is the relationship between the forest stand parameters (diameter at breast height, tree height, % cover) and the multi- polarised radar backscatter?

The relationship between the diameter at breast height and tree height and the cross polarised radar backscatter at long wavelength correlates was the strongest and most significant (r = 0.658, 0.543) in natural forest) while other polarisation showed strongest correlation with crown cover percentage (r = 0.526). Like polarised radar backscatter at short wavelength had weaker correlation with the stand parameters (r =0.207, 0.320, 0.004 in natural forest).

How strong is the relationship between AGB and the multi-polarised radar backscatter?

The most significant and strongest correlation with AGB was with cross polarisation at long wavelength (r = 0.691).

How sensitive is the extracted backscatter value from radar imagery to its geometry in affecting the correlation with AGB biomass?

The geometric sensitivity of the extracted backscatter value from radar imagery was a factor affecting the correlation with AGB biomass. In 1,4 and 9 pixels closest to the center of the plot, taking the 9 pixels setup showed best correlation with AGB (L-band HH: r =0.447, L-band HV: r = 0.878) .

Is the fused data of optical and radar images correlated with ABG biomass?

Fused data of optical and radar images did not show any strong correlation with AGB (highest in plantation with r = 0.529 with band B).

How accurate can the AGB in this study area be estimated using polarised radar backscatter by regression model?

AGB in the study area could not be estimated accurately for all land cover types. Only the AGB in the natural forest could be estimated and mapped accurately using multi linear regression of L-band HH and HV polarisation. Neither in plantation nor agro-forestry, a correlation with radar backscatter was strong enough to be used for estimation.

Can forest biomass and carbon stocks be mapped using radar images?

As the carbon stock was calculated from AGB, this research was in line with previous studies to prove the usefulness of radar imagery in mapping AGB and carbon stock. Furthermore, with multi-temporal radar images, the carbon sequestration assessment also could be mapped accurately. This will contribute to improve the knowledge of human about global carbon budget and its changes over the years, especially in tropical ecosystems where still remaining uncertainties in accuracy and cost.

Nevertheless, the research still had some limitations due to the constraint of time, budget and field data. It is recommended that larger field dataset needs to be collected from the field in all three types of land cover with considering to different managements. Moreover, larger dataset of radar image in multi-temporal and multi – polarisation could be helpful to improve the correlation with AGB and estimate carbon sequestration. For instance, a ratio of L-band and C-band HV also could be useful to estimate AGB and overcome the saturation issue in radar image. In addition, forest canopy density also can be considered to improve the correlation of radar and AGB.

References

Abdikan, S., Sanli, F. B., Balcik, F. B. and Goksel, C. (2008). Fusion of SAR images (PALSAR and RADARSAT-1) with multispectral SPOT image: A comparative analysis of resulting images. Beijing ISPRS

Abrams, M. (1999). The Advanced Spaceborne Thermal Emission and Reflection Radiometer (ASTER): Data Products for the High Spatial Resolution Imager on NASA's EOS-AMI Platform. International Journal of Remote Sensing-USA Sep-1999.

Andersen, H.-E., Reutebuch, S. and McGaughey, R. (2006). Active remote sensing: 43-66.

Appiah, M., Blay, D., Damnyag, L., Dwomoh, F., Pappinen, A. and Luukkanen, O. (2009). Dependence on forest resources and tropical deforestation in Ghana. Environment, Development and Sustainability 11(3): 471-487.

Araújo, T. M., Higuchi, N. and Júnior, J. A. d. C. (1999). Comparison of formulae for biomass determination in a tropical rain forest site the state of Pará, Brazil. Forest Ecology and Management 177: 43-52.

Austin, J. M., Mackey, B. G. and Van Niel, K. P. (2003). Estimating forest biomass using satellite radar: an exploratory study in a temperate Australian Eucalyptus forest. Forest Ecology and Management 176(1-3): 575-583.

Balzter, H. (2001). Forest mapping and monitoring with interferometric synthetic aperture radar (InSAR). Progress in Physical Geography 25.

Basuki, T. M., Laake, P. E. v., Skidmore, A. K. and Hussin, Y. A. (2009). Allometric equations for estimating the above- ground biomass in tropical lowland Dipterocarp forests Forest Ecology and Management 257.

Beaudoin, A., Le Toan, T., Goze, S., Nerzy, E. and Lopes, A. (1994). Retrieval of forest biomass from SAR data. International Journal of Remote Sensing 15(414).

Blackburn, G. A. and Steele, C. M. (1999). Towards the Remote Sensing of Matorral Vegetation Physiology: Relationships between Spectral Reflectance, Pigment, and Biophysical Characteristics of Semiarid Bushland Canopies. Remote Sensing of Environment 70(3): 278-292.

Blay, D., Appiah, M., Damnyag, L., Dwomoh, F. K., Luukkanen, O. and Pappinen, A. (2007). Involving local farmers in rehabilitation of degraded tropical forests: Some lessons from Ghana. Environment, Development and Sustainability.

Brown, I. F., Martinell, L. A., Thomas, W. W., Moreirac, M. Z., Cid Ferreirae, C. A. and Reynaldo, A. V. (1995). Uncertainty in the biomass of Amazonian forests: An example from Rondonia, Brazil. Forest Ecology and Management 75.

Brown, S. (1997). Estimating biomass and biomass change of tropical forests : a primer. Rome, FAO.

Brown, S. (2002). Measuring carbon in forests: current status and future challenges. Environmental Pollution 116(3): 363-372.

Brown, S., Gillespie, A. J. R. and Lugo, A. E. (1989). Biomass Estimation Methods for Tropical Forests with Applications to Forest Inventory Data. Forest Science 35: 881-902.

Cairns, M. A., Olmsted, I., Granados, J. and Argaez, J. (2003). Composition and aboveground tree biomass of a dry semi-evergreen forest on Mexico's Yucatan Peninsula. Forest Ecology and Management 186(1-3): 125-132.

Calvatildeo, T. and Palmeirim, J. M. (2004). Mapping Mediterranean scrub with satellite imagery: biomass estimation and spectral behaviour. International Journal of Remote Sensing 25: 3113-3126.

Carver, K. R., Cimino, J. B., Elaschi, C., Syvertson, M., Beal, R., Engman, T., Schaber, G., Ulaby, F. T., Weeks, W., CAmpbell, W., Carsey, F., Curlander, J. C., Dobsone, C., Fu, L., Gurney, R., Holt, B., Murphy, R., Schuman, R., Swift, C., Taranik, J., Wickland, D. and Zinkle, P. (1988). SAR Synthetic Aperture RADAR – Earth Observing System. NASA Instrument Panel Report. Washington D.C. IIf.

Castel, T., Guerra, F., Caraglio, Y. and Houllier, F. (2002). Retrieval biomass of a large Venezuelan pine plantation using JERS-1 SAR data. Analysis of forest structure impact on radar signature. Remote Sensing of Environment 79(1): 30-41.

Chambers, J. Q., Santos, J. d., Ribeiro, R. J. and Higuchi, N. (2001). Tree damage, allometric relationships, and above-ground net primary production in central Amazon forest. Forest Ecology and Management 152(1-3): 73-84.

Chave, J., Andalo, C., Brown, S., Cairns, M., Chambers, J., Eamus, D., Fölster, H., Fromard, F., Higuchi, N., Kira, T., Lescure, J. P., Nelson, B., Ogawa, H., Puig, H., Riéra, B. and Yamakura, T. (2005). Tree allometry and improved estimation of carbon stocks and balance in tropical forests. Oecologia 145(1): 87-99.

Chave, J., Condit, R., Salomon, A., Hernandez, A., Lao, S. and Perez, R. (2004). Error Propagation and Scaling for Tropical Forest Biomass Estimates. Philosophical Transactions: Biological Sciences 359(1443): 409-420.

Chen, D., Stow, D. A. and Gong, P. (2004). Examining the effect of spatial resolution and texture window size on classification accuracy: an urban environment case. International Journal of Remote Sensing 25: 2177-2192.

Chen, J., Brosofske, K., Noormets, A., Crow, T. R., Bresee, M. K., Le Moine, J., M. Euskirchen, E., Mather, S. V. and Zheng, D. (2003). A Working Framework for Quantifying Carbon Sequestration in Disturbed Land Mosaics. Environmental Management: 24.

CPF (2008). Strategic Framework for Forests and Climate Change- a proposal by Collaborative Partnership on Forests for a coordinated forest -sector response to climate change.

Cronin, N. L. R. (2004). The potential of airborne polarimetric systhetic aparture radar data for quantifying and mapping the biomass and structural diversity of woodlands in semi arid australia. School of Biological, Earth and Environmental Sciences, The University of New South Wales: 386.

Culvenor, D. S. (2003). Extracting individual tree information: a survey on techniques for high spatial resolution imagery. Boston, Kluwer Academic.

Curlander, J. C. and McDonough, R. N. (1991). Synthetic Aperture Radar: Systems and Signal Processing, J. Wiley & Sons, New York

de Gier, A. (2003). New approach to woody biomass assessment in woodlands and shrublands. Geoinformatics for tropical ecosystems

De Jong, S. M., Pebesma, E. J. and Lacaze, B. (2003). Above-ground biomass assessment of Mediterranean forests using airborne imaging spectrometry: the DAIS Peyne experiment. International Journal of Remote Sensing 24(7): 1505-1520.

Dobson, C., Ulaby, F. T. and Pierce, L. E. (1995). Estimation of forest biophysical characteristics in northern Michigan with SIR-C/X-SAR. IEEE Transactions on GeoScience and Remote Sensing 33.

Dobson, M. C., Ulaby, F. T., Le Toan, T., Beaudoin, A., Kasischke, E. S. and Christensen, M. (1992). Dependence of radar backscatter on conifer forest biomass. IEEE TRANSACTIONS ON GEOSCIENCE AND REMOTE SENSING 30(2): 412-415.

Dong, J., Zhuang, D., Huang, Y. and Fu, J. (2009) Advances in Multi-sensor data fusion: Algorithms and applications. 9, 7771-7784 DOI: 10.3390/s91007771.

Drake, J. B., Dubayah, R. O., Clark, D. B., Knox, R. G., Blair, J. B., Hofton, M. A., Chazdon, R. L., Weishampel, J. F. and Prince, S. (2002). Estimation of tropical forest structural characteristics using large-footprint lidar. Remote Sensing of Environment 79(2-3): 305-319.

Drake, J. B., Dubayah, R. O., Knox, R. G., Clark, D. B. and Blair, J. B. (2002). Sensitivity of large-footprint lidar to canopy structure and biomass in a neotropical rainforest. Remote Sensing of Environment 81(2-3): 378-392.

Elvidge, C. D. and Chen, Z. (1995). Comparison of broad-band and narrow-band red and near-infrared vegetation indices. Remote sensing of environment 54(1): 38-48.

FAO (2000). Global Forest Resources Assessment 2000-Main report.

FAO. (2003). WRB Map of World Soil Resources. from http://www.fao.org/ag/agl/agll/wrb/soilres.stm.

FAO (2004). Global forest resources assessment update 2005_Terms and definitions.

Fazakas, Z., Nilsson, M. and Olsson, H. (1999). Regional forest biomass and wood volume estimation using satellite data and ancillary data. Agricultural and Forest Meteorology 98-99: 417-425.

Fernandez, M. Q. (2002). Polarimetric data for tropical forest monitoring studies at the Colombian Amazon The Netherland, Wageningen University: 160.

Foody, G. M. (2003). Remote sensing of tropical forest environments: towards the monitoring of environmental resources for sustainable development. International Journal of Remote Sensing 24(20): 4035-4046.

Foody, G. M., Cutler, M. E., McMorrow, J., Pelz, D., Tangki, H., Boyd, D. S. and Douglas, I. (2001). Mapping the biomass of Bornean tropical rain forest from remotely sensed data. Global Ecology and Biogeography 10(4): 379-387.

Frank Rosillo-Calle, Peter de Groot, Sarah L. Hemstock and Woods, J. (2007). The Biomass Assessment Handbook. London, Earthscan.

Fujisada, H. (1994). Overview of ASTER instrument on EOS-AM1 platform, SPIE.

Gibbs, H. K., Brown, S., Niles, J. O. and Foley, J. A. (2007). Monitoring and estimating tropical forest carbon stocks: making REDD a reality. Environmental Research Letters 2(4): 045023.

Halme, M. and Tomppo, E. (2001). Improving the accuracy of multisource forest inventory estimates by reducing plot location error- a multicriteria approach. Remote Sensing of Environment 78: 321-327.

Harrell, P. A., Kasischke, E. S., Bourgeau-Chavez, L. L., Haney, E. and Christensen, N. L. (1997). Comparison of approaches to estimate of aboveground biomass in southern pine forests using SIR-C data. Remote Sensing of Environment 59: 223-233.

Henderson, F. M. e. and Lewis, A. J. e. (1998). Principles and applications of imaging radar. New York etc., Wiley & Sons.

Hoekman, D. H. (1990). Radar remote sensing data for applications in forestry, Wageningen Agricultural University: 279.

Hoekman, D. H., van de Sanden, J. and W, B. (1996). Radar remote sensing of tropical rain forest : The AIRSAR-93 campaign in Guyana and Columbia. Deft: 59.

Holopainen, M., Tuominen, S., Karjalainen, M., Hyyppa, J., Vastaranta, M. and Hyyppa, H. (2009). Accuracy of high resolution radar images in the estimation of plot level forest variables. Advances in GIScience. M. S. e. al., Springer- Verlag Berlin Heidelberg.

Houghton, R. A., Lawrence, K. T., Hackler, J. L. and Brown, S. (2001). The spatial distribution of forest biomass in the Brazilian Amazon: a comparison of estimates. Global Change Biology 7(7): 731-746.

Husch, B., Beers, T. W. and Kershaw, J. A. (2003). Forest mensuration. Hoboken, Wiley & Sons.

Hussin, Y. A. (1990). effects of polarization and incidence angle on radar backscatter from forest cover. PhD thesis Colorado State University; Summary in English. Fort Collins, Colorado State University: 187.

Hussin, Y. A., Reich, R. M. and Hoffer, R. M. (1991). Estimating splash pine biomass using radar backscatter. Geoscience and Remote Sensing, IEEE Transactions on 29(3): 427-431.

Hussin, Y. A., Reich, R. M. and Hoffer, R. M. (1992). Effect of polarization on radar backscatter in relation to slash pine stand biomass using aircraft and SIR - B data. In: ISPRS 1992 : Vol. 29 : Part B7, commission VII, pp. 661-667.

Hyde, P., Dubayah, R., Peterson, B., Blair, J. B., Hofton, M., Hunsaker, C., Knox, R. and Walker, W. (2005). Mapping forest structure for wildlife habitat analysis using waveform lidar: Validation of montane ecosystems. Remote Sensing of Environment 96(3-4): 427-437.

IPCC, Ed. (2003). Good Practice Guidance for Land Use Land-Use Change and Forestry.

IPCC (2006). Guideline for national Green House gas inevtories_Volume3.

IPCC (2006). Guideline for national Green House gas inventories_Volume4_ Agriculture, Forestry and Other Land Use.

Jensen, J. R. (2000). Remote sensing of the Environment: An Earth Resource Perspective, Prentice Hall.

Kasischke, E. S., Bourgeau-Chavez, L. L., Christensen, N. L. and Haney, E. (1994). Observations on the sensitivity of ERS-1 SAR image intensity to changes in aboveground biomass in young loblolly pine forests. International Journal of Remote Sensing 15(1): 3 - 16.

Kasischke, E. S. and Christensen, N. L. J. (1990). Connecting forest ecosystem and microwave backscatter models. International Journal of Remote Sensing 11(7): 1277-1298.

Kasischke, E. S., Melack, J. M. and Craig Dobson, M. (1997). The use of imaging radars for ecological applications--A review. Remote Sensing of Environment 59(2): 141-156.

Ketterings, Q. M., Coe, R., van Noordwijk, M., Ambagau, Y. and Palm, C. A. (2001). *Reducing uncertainty in the use of allometric biomass equations for predicting above-ground tree biomass in mixed secondary forests. Forest Ecology and Management 146(1-3): 199-209.*

Kurvonen, L., Pulliainen, J. and Hallikainen, M. (1999). *Retrieval of biomass in boreal forests from multitemporal ERS-1 and JERS-1 SAR images. IEEE TRANSACTIONS ON GEOSCIENCE AND REMOTE SENSING 37(1): 198-205.*

Le Toan, T., Beaudoin, A., Riom, J. and Guyon, D. (1992). *Relating forest biomass to SAR data. Geoscience and Remote Sensing, IEEE Transactions on 30(2): 403-411.*

Leckie, D. G. and Ranson, K. J. (1998). *Forestry applications using imaging radar. Principles and Applications of Imaging Radar. 2: 435-509.*

Lefsky, M. A., Cohen, W. B., Acker, S. A., Parker, G. G., Spies, T. A. and Harding, D. (1999). *Lidar Remote Sensing of the Canopy Structure and Biophysical Properties of Douglas-Fir Western Hemlock Forests. Remote Sensing of Environment 70(3): 339-361.*

Lefsky, M. A., Harding, D., Cohen, W. B., Parker, G. and Shugart, H. H. (1999). *Surface Lidar Remote Sensing of Basal Area and Biomass in Deciduous Forests of Eastern Maryland, USA. Remote Sensing of Environment 67(1): 83-98.*

Lévesque, J. and King, D. J. (2003). *Spatial analysis of radiometric fractions from high-resolution multispectral imagery for modelling individual tree crown and forest canopy structure and health. Remote Sensing of Environment 84(4): 589-602.*

Lillesand, T. M., Kiefer, R. W. and Chipman, J. W. (2004). *Remote sensing and image interpretation. New York, Wiley & Sons.*

Lovell, J., Jupp, D., Culvenor, D. and Coops, N. (2003). *Using airborne and ground based ranging Lidar to measure canopy structure in Australian forests. Canadian Journal of Remote Sensing 29: 607-622.*

Lu, D. (2006). *The potential and challenge of remote sensing-based biomass estimation. International Journal of Remote Sensing 27(7): 1297 - 1328.*

Lu, D. and Batistella, M. (2005). *Exploring TM image texture and its relationships with biomass estimation in Rondônia, Brazilian Amazon. Acta Amazonica 35: 249-257.*

Lu, D., Batistella, M. and Moran, E. (2005). *Satellite Estimation of Aboveground Biomass and Impacts of Forest Stand Structure. Photogrammetric Engineering & Remote Sensing 71(8): 967–974.*

Lu, D., Mausel, P., Brondízio, E. and Moran, E. (2004). *Relationships between forest stand parameters and Landsat TM spectral responses in the Brazilian Amazon Basin. Forest Ecology and Management 198(1-3): 149-167.*

Luckman, A., Baker, J., Kuplich, T. M., da Costa Freitas Yanasse, C. and Frery, A. C. (1997). *A study of the relationship between radar backscatter and regenerating tropical forest biomass for spaceborne SAR instruments. Remote Sensing of Environment 60(1): 1-13.*

Luckman, A., Baker, J. R., Honzak, M. and Lucas, R. (1998). *Tropical Forest Biomass Density Estimation using JERS-1 SAR : Seasonal Variation, Confidence Limits and Application to Image Mosaics. Remote Sensing of Environment 63: 126-139.*

Mickler, R. A., Earnhardt, T. S. and Moore, J. A. (2002). *Regional estimation of current and future forest biomass. Environmental Pollution 116.*

Mutanga, O. and Skidmore, A. K. (2004). *Narrow band vegetation indices overcome the saturation problem in biomass estimation. International Journal of Remote Sensing 25: 3999-4014.*

Næsset, E. (1997). *Determination of mean tree height of forest stands using airborne laser scanner data. ISPRS Journal of Photogrammetry and Remote Sensing 52(2): 49-56.*

Næsset, E. (1997). *Estimating timber volume of forest stands using airborne laser scanner data. Remote Sensing of Environment 61(2): 246-253.*

Nelson, B. W., Mesquita, R., Pereira, J. L. G., Garcia Aquino de Souza, S., Teixeira Batista, G. and Bovino Couto, L. (1999). *Allometric regressions for improved estimate of secondary forest biomass in the central Amazon. Forest Ecology and Management 117(1-3): 149-167.*

Nelson, R. F., Kimes, D. S., Salas, W. A. and Routhier, M. (2000). *Secondary Forest Age and Tropical Forest Biomass Estimation Using Thematic Mapper Imagery. BioScience 50(5): 13.*

Nilsson, M. (1996). *Estimation of tree heights and stand volume using an airborne lidar system. Remote Sensing of Environment 56(1): 1-7.*

Patenaude, G., Milne, R. and Dawson, T. P. (2005). Synthesis of remote sensing approaches for forest carbon estimation: reporting to the Kyoto Protocol. Environmental Science & Policy 8(2): 161-178.

PCI-Geomatics. (2009). Focus on radar. Retrieved 05/02/2010, from http://www.pcigeomatics.com/pdfs/radar_focus_on.pdf.

Phua, M.-H. and Saito, H. (2003). Estimation of biomass of a mountainous tropical forest using Landsat TM data. Canadian Journal of Remote Sensing 29(4).

Pohl, C. and Van Genderen, J. L. (1998). Review article Multisensor image fusion in remote sensing: concepts, methods and applications. International Journal of Remote Sensing 19(5): 823 - 854.

Pulliainen, J. T., P.J. Mikkela, M.T. Hallikainen, and J.-P. Ikonen (1996). Seasonal dynamics of C-band backscatter of boreal forests with applications to biomass and soil moisture. IEEE TRANSACTIONS ON GEOSCIENCE AND REMOTE SENSING 34: 758-770.

Ranson, K. J. and Sun, G. (1994). Mapping biomass of a northern forest using multifrequency SAR data. Geoscience and Remote Sensing, IEEE Transactions on 32(2): 388-396.

Ranson, K. J. and Sun, G. (1994). Mapping Biomass of a Northern Forest Using Multifrequency SAR data. IEEE Transactions on GeoScience and Remote Sensing 32(2).

Rauste, Y., Hammer, T., Pulliainen, J. and Hallikainen, M. (1994). Radar-based forest biomass estimation. International journal of remote sensing 15(14): 2791-2808.

Rauste, Y., Heiska, K. and Pulliainen, J. (1992). On forest inventory and elevation determination using polarimetric radar data. Proceedings of the Final Workshop of the MAESTRO/AGRISCATT Campaigns, Noordwijk, 6–7 March 1992 117–121.

Richards, J. A. and Jia, X. (2006). Remote Sensing Digital Image Analysis - an introduction. Canberra, Springer.

Rosenqvist, A., Imhoff, M., Milne, A. and Dobson, C. (1999). Remote Sensing and the Kyoto Protocol: A Review of Available and Future Technology for Monitoring Treaty Compliance. Ann Arbon, Michigan, USA.

Rosenqvist, A., Shimada, M., Igarashi, T., Watanabe, M., Tadono, T. and Yamamoto, H. (2003). Support to multi-national environmental conventions and terrestrial carbon cycle science by ALOS and ADEOS-II -the Kyoto & carbon initiative. Geoscience and Remote Sensing Symposium, 2003. IGARSS '03. Proceedings. 2003 IEEE International.

Rosenqvist, Å. M., Anthony Lucas, Richard Imhoff and Marc Dobson, C. (2003). A review of remote sensing technology in support of the Kyoto Protocol. Environmental Science & Policy 6(5): 441-455.

Rosich, B. and Meadows, P. (2004). Absolute calibration of ASAR level 1 products generated with PF-ASAR, ESA.

Rosillo-Calle, F., de Groot, P., Hemstock, S. L. and Woods, J. (2007). The Biomass Assessment Handbook. London, Earthscan.

Roy, P. S. and Ravan, S. A. (1996). Biomass estimation using satellite remote sensing data - An investigation on possible approaches for natural forest. Journal of Biosciences 21(4): 535-561.

Sader, S. A., Waide, R. B., Lawrence, W. T. and Joyce, A. T. (1989). Tropical forest biomass and successional age class relationships to a vegetation index derived from Landsat TM data. . Remote Sensing of Environment 28: 143-156.

Santos, J. R., Araujo, L. S., Freitas, C. C., Dutra, L. V., Sant'Anna, S. J. S., Kuplich, T. M. and Gama, F. F. (2003). Allometric equations for tropical forest estimation and its relationship with P-band SAR data. Geoscience and Remote Sensing Symposium, 2003. IGARSS '03. Proceedings. 2003 IEEE International.

Santos, J. R., Freitas, C. C., Araujo, L. S., Dutra, L. V., Mura, J. C., Gama, F. F., Soler, L. S. and Sant'Anna, S. J. S. (2003). Airborne P-band SAR applied to the aboveground biomass studies in the Brazilian tropical rainforest. Remote Sensing of Environment 87(4): 482-493.

Santos, J. R., Lacruz, M. S. P., Araujo, L. S. and Keil, M. (2002). Savanna and tropical rainforest biomass estimation and spatialization using JERS-1 data. International Journal of Remote Sensing 23(7): 1217-1229.

Schoene, D., Killmann, W., Lüpke, H. v. and LoycheWilkie, M. (2007). Definitional issues related to reducing emissions from deforestation in developing countries. Forests and Climate Change Working Paper 5. FAO. Rome.

Scott, J. G., Baccini, A., Nadine T Laptorte, Tracy Johns, Wayne Walker, Josef Kellndorfer, Houghton, R. A. and Sun, M. (2009). Mapping and monitoring carbon stocks with sattelite observations: a comparison of methods. Carbon Balance and Management.

Shimada, M., Isoguchi, O., Tadono, T. and Isono, K. (2009). PALSAR Radiometric and Geometric Calibration. IEEE TRANSACTIONS ON GEOSCIENCE AND REMOTE SENSING 47(12): 3915-3932.

Sierra, C. A., del Valle, J. I., Orrego, S. A., Moreno, F. H., Harmon, M. E., Zapata, M., Colorado, G. J., Herrera, M. A., Lara, W., Restrepo, D. E., Berrouet, L. M., Loaiza, L. M. and Benjumea, J. F. (2007). Total carbon stocks in a tropical forest landscape of the Porce region, Colombia. Forest Ecology and Management 243(2-3): 299-309.

Spurr, S. H. (1952). Forest inventory. New York, The Ronald Press.

Stein, A. e., van der Meer, F. D. e. and Gorte, B. G. H. e. (1999). Spatial statistics for remote sensing. Dordrecht, Kluwer Academic.

Steininger, M. K. (2000). Satellite estimation of tropical secondary forest above-ground biomass: data from Brazil and Bolivia. International Journal of Remote Sensing 21(6): 1139 - 1157.

Thenkabail, P. S., Enclona, E. A., Ashton, M. S., Legg, C. and De Dieu, M. J. (2004). Hyperion, IKONOS, ALI, and ETM+ sensors in the study of African rainforests. Remote Sensing of Environment 90(1): 23-43.

Tiwari, A. K. and Singh, J. S. (1984). Mapping forest biomass in India through aerial photographs and nondestructive field sampling. Applied Geography 4(2): 151-165.

Treitz, P. M. and Howarth, P. J. (1999). Hyperspectral remote sensing for estimating biophysical parameters of forest ecosystems. Progress in Physical Geography 23(3): 359-390.

Ulaby, F. T., Sarabandi, K., McDonald, K., Whitt, M. and Dobson, M. C. (1990). Michigan microwave canopy scattering model. International Journal of Remote Sensing 11(7): 1223-1253.

UNFCC (2008). Report of the Conference of the Parties on its thirteenth session, held in Bali from 3 to 15 December 2007.

Ustin, S. L. e. (2004). Remote sensing for natural resource management and environmental monitoring. Hoboken etc., Wiley & Sons.

Van der Sanden, J. (1997). Radar remote to support tropical forest management Wagenignen, University of Wagenignen.

Vega, B., Hussin, Y. A. and Sharifi, M. A. (2006). Optical and microwave image fusion to detect and monitor illegal logging and tropical rain forest encroachment in East Kalimantan, Indonesia. In: ACRS 2006 : Proceedings of the 27th Asian conference on remote sensing ACRS, 9-13 October, 2006 Ulanbaatar, Mongolia. Bangkok : Asian Association of Remote Sensing (AARS), 2006. 6 p.

Vine, E., Sathaye, J. and Makundi, W. (1999). Guidelines for the Monitoring, Evaluation, Reporting, Verification, and Certification of Forestry Projects for Climate Change Mitigation, Lawrence Berkeley National Laboratory: Lawrence Berkeley National Laboratory. LBNL Paper LBNL-41877. Retrieved from: http://www.escholarship.org/uc/item/20h2r692.

Wu, S. T. (1990). Assessment of tropical forest stand characteristics with multipolarization SAR data acquired over a mountainous region in Costa Rica. IEEE Transactions on GeoScience and Remote Sensing 28(4).

Wu, S. T. and Sader, S. A. (1987). Multipolarization SAR Data for Surface Feature Delineation and Forest Vegetation Characterization. Geoscience and Remote Sensing, IEEE Transactions on GE-25(1): 67-76.

Wulder, M. (1998). Optical remote-sensing techniques for the assessment of forest inventory and biophysical parameters. Progress in Physical Geography 22(4): 449-476.

Zheng, D., Rademacher, J., Chen, J., Crow, T., Bresee, M., Le Moine, J. and Ryu, S.-R. (2004). Estimating aboveground biomass using Landsat 7 ETM+ data across a managed landscape in northern Wisconsin, USA. Remote Sensing of Environment 93(3): 402-411.

Zimble, D. A., Evans, D. L., Carlson, G. C., Parker, R. C., Grado, S. C. and Gerard, P. D. (2003). Characterizing vertical forest structure using small-footprint airborne LiDAR. Remote Sensing of Environment 87(2-3): 171-182.

Appendix A - List of local tree species

Local name	Scientific name
Akye	*Blighia sapida*
Emire	*Terminalia ivorensis*
Esa	*Celtis mildbraesii*
Esia	*Petersianthus spp.*
Foto	*Glyphaea brevis*
Funtum	*Funtumia elastic*
Kakadukro	*Trichilia prieuriana*
Kyenkyen	*Antiaris toxicaria*
Mahogani	*Khaya grandisfoliola*
Mansonia	*Mansonia altissima*
Nyankyerene	*Ficus exasperate*
Ofram	*Terminalia superb*
Okoro	*Albizia zygia*
Odum	*Milicia excels*
Onyina	*Ceiba pentandra*
Prekese	*Tetrapleura tetraptera*
Sese	*Holarrhena floribunda*
Watapuo	*Cola gigantean*
wawa	*Trilochiton scleroxylon*
Wawabema	*Sterculia rhinopetala*
Wonton	*Morus mesozygia*

Appendix B- ALOS PALSAR calibration accuracy

Items	Measured value		No of data	Specification
Geometric accuracy	9.7 m (RMS): STRIP mode		572	100m
	70 m (RMS): SCANSAR			
Radiometric accuracy	0.219 dB (1 sigma) from Amazon forest		572	1.5dB
	0.76dB (1sigma) from CRs			1.5dB
	0.17 dB (1 sigma: Sweden CSs)			1.5dB
	-34 dB (Noise equivalent Sigma-zero for HV)			-23 dB
	-32 dB (as a minimum of FBD-HH)			
	-29 dB (as a minimum of FBS-HH)			
Polarimetric calibration	VV/HH ratio	1.013(0.062)*	81	0.2 dB
	VV/HH phase diff	0.612deg(2.66)		5deg
	Cross talk	-31.7 (4.3)		-30 dB
Resolution	Azimuth	4.49m (0.1)*	572	-4.5m
	Range (14MHz)	9.06m (0.1m)		10.7m
	Range (28MHz)	4.7m (0.1m)		5.4m
Side slope	PSLR in azimuth	-16.6 dB	572	-10dB
	PSLR in range	-12.6 dB		-10dB
	ISLR	-8.6 dB		-8 dB
Ambiguity	Azimuth	Not appear		16 dB
	Range	23 dB		16 dB
Transmission power	Sum of 80 TRM	2220W		2000W

A(B)* represents an average value of A and a standard deviation of (B)

PSLR is Peak-to-Side-Slope Ratio and ISLR is Integrated Side-Lobe Ratio

Appendix C – Photos from the field

C1- Natural Forest

C2- Plantation

C3- Agro-forestry

C4- Transportation vehicle and accessibility

C5- Popular Crops in taungya system

Appendix D : Correlation of forest stand parameters and radar backscatter in different land cover types

D1- Natural forest

Correlations

		Height	HH
Height	Pearson Correlation	1.000	-.454
	Sig. (2-tailed)		.089
	N	15	15
HH	Pearson Correlation	-.454	1.000
	Sig. (2-tailed)	.089	
	N	15	15

Correlations

		Height	HV
Height	Pearson Correlation	1.000	-.543*
	Sig. (2-tailed)		.036
	N	15	15
HV	Pearson Correlation	-.543*	1.000
	Sig. (2-tailed)	.036	
	N	15	15

*. Correlation is significant at the 0.05 level (2-tailed).

Correlations

		Height	C_HH
Height	Pearson Correlation	1.000	.320
	Sig. (2-tailed)		.245
	N	15	15
C_HH	Pearson Correlation	.320	1.000
	Sig. (2-tailed)	.245	
	N	15	15

Correlations

		crown_cover	HH
crown_cover	Pearson Correlation	1.000	-.527*
	Sig. (2-tailed)		.044
	N	15	15
HH	Pearson Correlation	-.527*	1.000
	Sig. (2-tailed)	.044	
	N	15	15

*. Correlation is significant at the 0.05 level (2-tailed).

Correlations

		crown_cover	HV
crown_cover	Pearson Correlation	1.000	-.324
	Sig. (2-tailed)		.239
	N	15	15
HV	Pearson Correlation	-.324	1.000
	Sig. (2-tailed)	.239	
	N	15	15

Correlations

		crown_cover	C_HH
crown_cover	Pearson Correlation	1.000	-.014
	Sig. (2-tailed)		.961
	N	15	15
C_HH	Pearson Correlation	-.014	1.000
	Sig. (2-tailed)	.961	
	N	15	15

Correlations

		Average_DBH	HH
Average_DBH	Pearson Correlation	1.000	.046
	Sig. (2-tailed)		.870
	N	15	15
HH	Pearson Correlation	.046	1.000
	Sig. (2-tailed)	.870	
	N	15	15

Correlations

		Average_DBH	HV
Average_DBH	Pearson Correlation	1.000	.659**
	Sig. (2-tailed)		.008
	N	15	15
HV	Pearson Correlation	.659**	1.000
	Sig. (2-tailed)	.008	
	N	15	15

**. Correlation is significant at the 0.01 level (2-tailed).

Correlations

		Average_DBH	C_HH
Average_DBH	Pearson Correlation	1.000	-.208
	Sig. (2-tailed)		.457
	N	15	15
C_HH	Pearson Correlation	-.208	1.000
	Sig. (2-tailed)	.457	
	N	15	15

D2-Plantation

Correlations

		HH_central	Height
HH_central	Pearson Correlation	1.000	.023
	Sig. (2-tailed)		.934
	N	15	15
Height	Pearson Correlation	.023	1.000
	Sig. (2-tailed)	.934	
	N	15	15

Correlations

		Height	HV_central
Height	Pearson Correlation	1.000	.009
	Sig. (2-tailed)		.974
	N	15	15
HV_central	Pearson Correlation	.009	1.000
	Sig. (2-tailed)	.974	
	N	15	15

Correlations

		Height	HH_Envisat
Height	Pearson Correlation	1.000	-.155
	Sig. (2-tailed)		.580
	N	15	15
HH_Envisat	Pearson Correlation	-.155	1.000
	Sig. (2-tailed)	.580	
	N	15	15

Correlations

		HH_Envisat	cown_cover
HH_Envisat	Pearson Correlation	1.000	.185
	Sig. (2-tailed)		.509
	N	15	15
cown_cover	Pearson Correlation	.185	1.000
	Sig. (2-tailed)	.509	
	N	15	15

Correlations

		cown_cover	HH_central
cown_cover	Pearson Correlation	1.000	-.169
	Sig. (2-tailed)		.548
	N	15	15
HH_central	Pearson Correlation	-.169	1.000
	Sig. (2-tailed)	.548	
	N	15	15

Correlations

		cown_cover	HV_central
cown_cover	Pearson Correlation	1.000	-.207
	Sig. (2-tailed)		.459
	N	15	15
HV_central	Pearson Correlation	-.207	1.000
	Sig. (2-tailed)	.459	
	N	15	15

Correlations

		HV_central	Average_DBH
HV_central	Pearson Correlation	1.000	.211
	Sig. (2-tailed)		.450
	N	15	15
Average_DBH	Pearson Correlation	.211	1.000
	Sig. (2-tailed)	.450	
	N	15	15

Correlations

		Average_DBH	HH_central
Average_DBH	Pearson Correlation	1.000	.094
	Sig. (2-tailed)		.738
	N	15	15
HH_central	Pearson Correlation	.094	1.000
	Sig. (2-tailed)	.738	
	N	15	15

Correlations

		Average_DBH	HH_Envisat
Average_DBH	Pearson Correlation	1.000	.361
	Sig. (2-tailed)		.187
	N	15	15
HH_Envisat	Pearson Correlation	.361	1.000
	Sig. (2-tailed)	.187	
	N	15	15

D3-Agroforestry

Correlations

		HH	Height
HH	Pearson Correlation	1.000	.143
	Sig. (2-tailed)		.398
	N	37	37
Height	Pearson Correlation	.143	1.000
	Sig. (2-tailed)	.398	
	N	37	37

Correlations

		Height	HV
Height	Pearson Correlation	1.000	.300
	Sig. (2-tailed)		.072
	N	37	37
HV	Pearson Correlation	.300	1.000
	Sig. (2-tailed)	.072	
	N	37	37

Correlations

		Height	HH_Envisat
Height	Pearson Correlation	1.000	-.055
	Sig. (2-tailed)		.746
	N	37	37
HH_Envisat	Pearson Correlation	-.055	1.000
	Sig. (2-tailed)	.746	
	N	37	37

D3-Agroforestry

Correlations

		HH	crown_cover
HH	Pearson Correlation	1.000	-.345*
	Sig. (2-tailed)		.036
	N	37	37
crown_cover	Pearson Correlation	-.345*	1.000
	Sig. (2-tailed)	.036	
	N	37	37

*. Correlation is significant at the 0.05 level (2-tailed).

Correlations

		crown_cover	HV
crown_cover	Pearson Correlation	1.000	-.111
	Sig. (2-tailed)		.514
	N	37	37
HV	Pearson Correlation	-.111	1.000
	Sig. (2-tailed)	.514	
	N	37	37

Correlations

		crown_cover	HH_Envisat
crown_cover	Pearson Correlation	1.000	-.166
	Sig. (2-tailed)		.325
	N	37	37
HH_Envisat	Pearson Correlation	-.166	1.000
	Sig. (2-tailed)	.325	
	N	37	37

Correlations

		Average_DBH	HH
Average_DBH	Pearson Correlation	1.000	-.205
	Sig. (2-tailed)		.224
	N	37	37
HH	Pearson Correlation	-.205	1.000
	Sig. (2-tailed)	.224	
	N	37	37

Correlations

		Average_DBH	HV
Average_DBH	Pearson Correlation	1.000	.163
	Sig. (2-tailed)		.335
	N	37	37
HV	Pearson Correlation	.163	1.000
	Sig. (2-tailed)	.335	
	N	37	37

Correlations

		Average_DBH	HH_Envisat
Average_DBH	Pearson Correlation	1.000	.203
	Sig. (2-tailed)		.228
	N	37	37
HH_Envisat	Pearson Correlation	.203	1.000
	Sig. (2-tailed)	.228	
	N	37	37